Article

Cell Reports

PROX1 Promotes Metabolic Adaptation and Fuels Outgrowth of Wnt^{high} Metastatic Colon Cancer Cells

Graphical Abstract

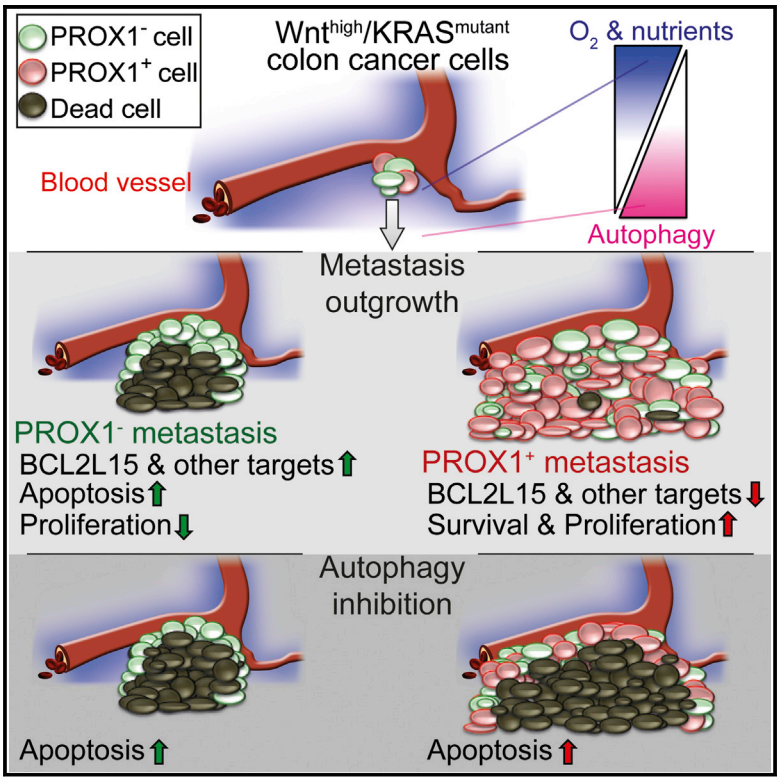

Highlights

PROX1 is expressed in stem-like/progenitor cell subpopulation in Wnt^{high} metastases

PROX1 promotes autophagy-dependent metabolic adaptation and apoptosis evasion

Genome-wide analyses identify direct PROX1 targets, such as pro-apoptotic BCL2L15

Authors

Simone Ragusa, Jianpin Cheng, ..., Mauro Delorenzi, Tatiana V. Petrova

Correspondence

tatiana.petrova@unil.ch

In Brief

Abnormal Wnt pathway activation is involved in the initiation of most colorectal cancers; however, little is known about its contribution to metastatic outgrowth. Ragusa et al. report that the Wnt target transcription factor PROX1 is produced in a subpopulation of colon cancer stem/progenitor cells and orchestrates the transcriptional network responsible for autophagy-dependent survival of metastases. Inactivation of PROX1 or PROX1-associated pathways prevents expansion of macrometastases and may provide new targets for therapeutic intervention in Wnt^{high} colorectal cancer.

Accession Numbers

E-MTAB-2020
E-MTAB-2021
GSE60390

Ragusa et al., 2014, Cell Reports 8, 1957–1973
September 25, 2014 ©2014 The Authors
http://dx.doi.org/10.1016/j.celrep.2014.08.041

Cell Reports
Article

PROX1 Promotes Metabolic Adaptation and Fuels Outgrowth of Wnt^{high} Metastatic Colon Cancer Cells

Simone Ragusa,[1] Jianpin Cheng,[1] Konstantin I. Ivanov,[1,12] Nadine Zangger,[4] Fatih Ceteci,[5] Jeremiah Bernier-Latmani,[1] Stavros Milatos,[1] Jean-Marc Joseph,[6] Stephane Tercier,[6] Hanifa Bouzourene,[7] Fredrik T. Bosman,[8] Igor Letovanec,[8] Giancarlo Marra,[9] Michel Gonzalez,[10] Patrizia Cammareri,[5] Owen J. Sansom,[5] Mauro Delorenzi,[1,4,11] and Tatiana V. Petrova[1,2,3,*]

[1]Department of Oncology, Centre Hospitalier Universitaire Vaudois (CHUV) and University of Lausanne, Lausanne 1066, Switzerland
[2]Department of Biochemistry, University of Lausanne, Lausanne 1066, Switzerland
[3]Swiss Institute for Cancer Research, EPFL, Lausanne 1015, Switzerland
[4]SIB Bioinformatics Core Facility, Swiss Institute of Bioinformatics, Lausanne 1015, Switzerland
[5]Cancer Research UK Beatson Institute, G61 1BD Glasgow, UK
[6]Service de Chirurgie Pédiatrique, Centre Hospitalier Universitaire Vaudois (CHUV), Lausanne 1011, Switzerland
[7]UNISciences, University of Lausanne, UniLabs, Lausanne 1066, Switzerland
[8]Institut Universitaire de Pathologie, CHUV, Lausanne 1011, Switzerland
[9]Institute of Molecular Cancer Research, University of Zurich, Zurich 8057, Switzerland
[10]Division of Thoracic Surgery, CHUV, Lausanne 1011, Switzerland
[11]Ludwig Center for Cancer Research, University of Lausanne, Lausanne 1066, Switzerland
[12]Present address: Department of Food and Environmental Sciences, University of Helsinki, Helsinki 00014, Finland
*Correspondence: tatiana.petrova@unil.ch
http://dx.doi.org/10.1016/j.celrep.2014.08.041

SUMMARY

The Wnt pathway is abnormally activated in the majority of colorectal cancers, and significant knowledge has been gained in understanding its role in tumor initiation. However, the mechanisms of metastatic outgrowth in colorectal cancer remain a major challenge. We report that autophagy-dependent metabolic adaptation and survival of metastatic colorectal cancer cells is regulated by the target of oncogenic Wnt signaling, homeobox transcription factor PROX1, expressed by a subpopulation of colon cancer progenitor/stem cells. We identify direct PROX1 target genes and show that repression of a pro-apoptotic member of the BCL2 family, BCL2L15, is important for survival of PROX1^{+} cells under metabolic stress. PROX1 inactivation after the establishment of metastases prevented further growth of lesions. Furthermore, autophagy inhibition efficiently targeted metastatic PROX1^{+} cells, suggesting a potential therapeutic approach. These data identify PROX1 as a key regulator of the transcriptional network contributing to metastases outgrowth in colorectal cancer.

INTRODUCTION

Colorectal cancer (CRC) is one of the leading causes of cancer-related mortality. The prognosis is especially poor for metastatic CRC, with overall 5-year survival rates of 5%–8% (Cunningham et al., 2010). Current treatment options include resection of solitary metastases and combinations of anti-vascular endothelial growth factor (VEGF) or epidermal growth factor receptor (EGFR) inhibitors and cytotoxic therapy. However, these targeted therapies are effective only in a small subset of patients with metastatic disease and treatment benefits are short-lived, further highlighting the need for a better understanding of metastatic CRC (De Roock et al., 2011).

Wnt signaling is essential for the maintenance of normal intestinal stem cells and is aberrantly activated in a significant proportion of CRCs (Clevers, 2013). The evolutionary conserved transcription factor PROX1 is a Wnt target gene in colon adenomas, where it contributes to the transition from early to dysplastic stage (Petrova et al., 2008). Prox1 is not expressed in normal intestinal stem cells, demonstrating that only oncogenic Wnt signaling triggers Prox1 expression (Petrova et al., 2008). Increased epithelial-to-mesenchymal transition (EMT) was recently reported in PROX1-expressing CRC cells in vitro (Lu et al., 2012). However, the role of PROX1 in metastatic CRC has not been investigated. Here, we report that PROX1 is expressed in stem-like cells in a subset of Wnt^{high} colon carcinomas and metastases. PROX1 acts as a key regulator of macrometastatic lesions outgrowth by promoting adaptation of tumor cells to hypoxia and nutrient deprivation. Furthermore, we show that targeting autophagy efficiently eliminates the growth advantage of PROX1^{+} cells. We identify direct PROX1 target genes in CRC cells and show that a pro-apoptotic member of BCL2 family, BCL2L15, is one of the downstream effectors of PROX1. Our data thus identify a cancer-specific component of the Wnt signaling required for outgrowth of metastases and suggest that inhibition of PROX1, or PROX1-regulated pathways, might constitute a new therapeutic approach.

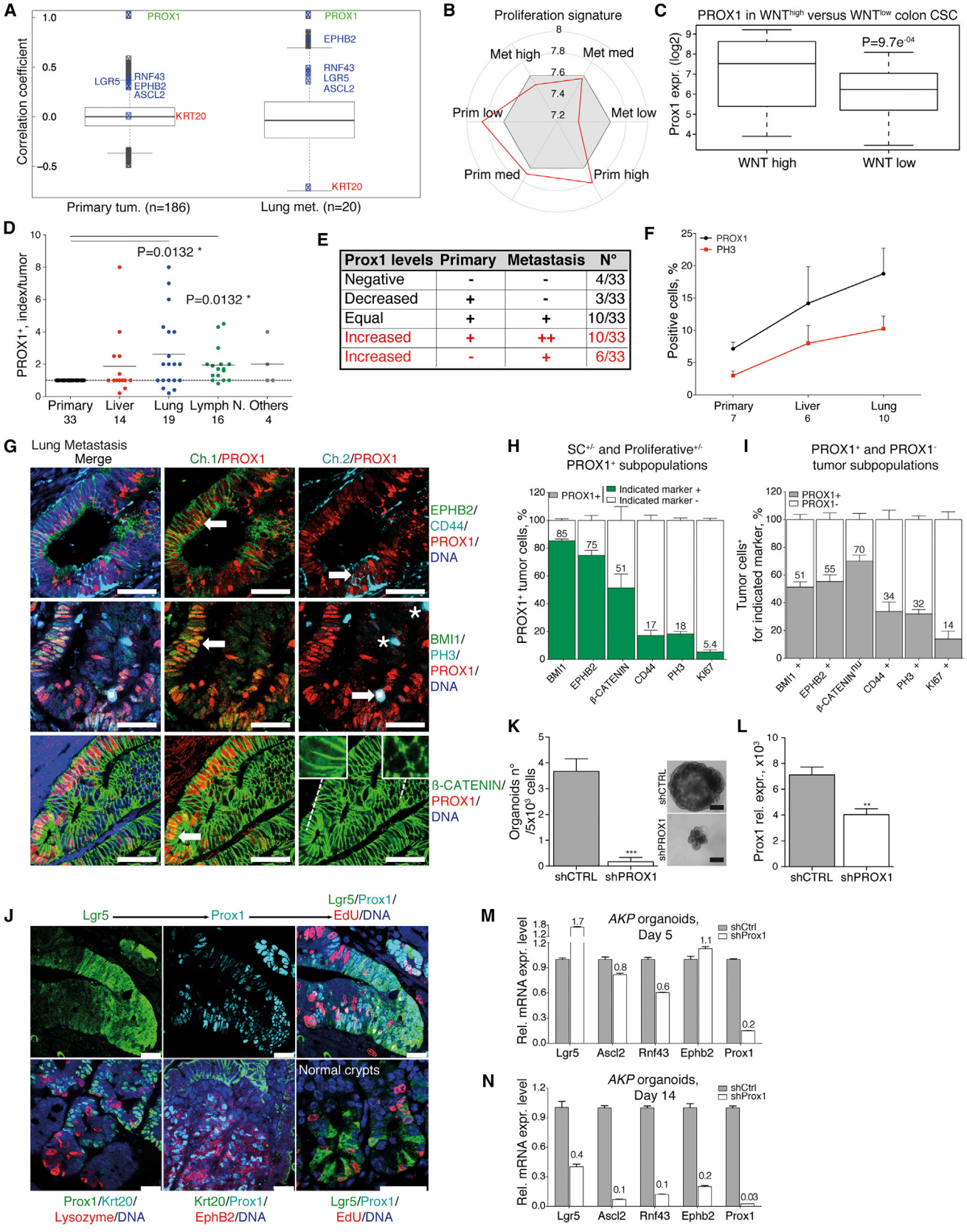

(legend on next page)

RESULTS

PROX1 Is Expressed in Progenitor/Stem Cells in Wnt^{high} Colon Cancer Metastases

We examined whether PROX1 expression correlates with Wnt signaling, stem-like/progenitor markers, cell differentiation, and proliferation, using transcriptomes of 166 primary CRCs and 20 lung metastases (Sheffer et al., 2009). PROX1 expression significantly correlated with stem/progenitor cell markers and Wnt targets LGR5, ASCL2, RNF43, and EPHB2 (Clevers, 2013) in primary tumors, and this correlation was further significantly increased in lung metastases (Figure 1A; $p < 0.05$). In contrast, PROX1 expression in metastases anticorrelated with the differentiation marker KRT20 (Figure 1A). Analysis of the proliferation signature MKI67, FOXM1, MYC, and AURKB (Jung et al., 2011) revealed that PROX1 levels did not correlate with the signature in primary tumors, whereas PROX1^{low} metastases had a lower proliferation index (Figure 1B).

We next asked how PROX1 expression correlates with molecular subtypes of CRC described by Budinska et al. (2013) and Sadanandam et al. (2013). Highest PROX1 levels were found in Wnt^{high} subtypes in both classification schemes (Figures S1A and S1B). In contrast, PROX1 was low in more-differentiated subtypes, such as the subtype A with high expression of differentiation markers and subtype C with high frequency of cancer-specific DNA hypermethylation (CIMP-H) of the Budinska et al. classification. Most of CIMP CRCs are also mismatch repair (MMR) deficient due to hypermethylation of the *MLH1* gene promoter (Truninger et al., 2005). In agreement with these results, PROX1 was low in MMR-deficient CRCs (Figures S1C–S1E). We further confirmed these data using the Pan-European Trials in Alimentary Tract Cancers database, containing microsatellite instability status analysis for 688 CRC primary colon carcinomas (Roth et al., 2010; Figure S1F).

The bioinformatics analysis predicted that PROX1 correlates with stem/progenitor markers, high Wnt signaling, and proliferation and anticorrelates with differentiation markers. Interrogation of transcriptomes from human CRC stem cells, stratified by the levels of Wnt signaling (de Sousa E Melo et al., 2011), demonstrated that PROX1 was significantly higher in Wnt^{high} versus Wnt^{low} cancer stem cells (Figure 1C; $p = 9.7 \times 10^{-4}$). To evaluate PROX1 protein levels in metastasis versus primary tumor, we stained 33 matched primary CRCs and their metastases. Lung and lymph node metastases had significantly higher levels of PROX1 in comparison to the primary tumors, with a positive trend for other metastatic sites (Figures 1D, 1E, and S1G). To establish whether PROX1 is expressed in stem/progenitor cells, we analyzed coexpression of PROX1 and EPHB2, CD44 and BMI1, previously shown to encompass progenitor/stem cell populations (Todaro et al., 2014; Martorell et al., 2014; Merlos-Suárez et al., 2011; Kreso et al., 2014). We also analyzed β-catenin nuclear/cytoplasmic localization as a marker of Wnt pathway activation, proliferation, and differentiation. In agreement with the bioinformatics analyses, differentiated KRT20$^+$ cells did not express PROX1 and, in metastases, cell proliferation correlated with levels of PROX1 (Figures 1F and S1H–S1J). The majority of PROX1$^+$ cells also coexpressed EPHB2 and BMI1, 50% had nuclear/cytoplasmic β-catenin, and 17% coexpressed CD44 or proliferation markers. A significant proportion of EPHB2$^+$, BMI1$^+$, CD44$^+$, and PH3$^+$ cells did not express PROX1 (Figures 1G–1I). Thus, in human metastases, PROX1 partially colocalizes with markers of stem/progenitor cells, proliferation, and activated WNT signaling.

To extend our observations to a model with a well-characterized stem cell compartment, we analyzed adenomas from *Apc$^{fl/fl}$;Lgr5-EGFP-Ires-CreERT2* mice. GFP marks Lgr5$^+$ normal and transformed stem cells, which give rise to differentiated progeny in both normal intestine and adenoma (Schepers et al., 2012). Fifty to sixty percent of GFP^{high}, GFP^{low}, EphB2$^+$, or proliferating 5-ethynyl-2′-deoxyuridine (EdU)$^+$ cells expressed Prox1, whereas Prox1 was absent in differentiated lysozyme$^+$ Paneth cells or Krt20$^+$ enterocytes (Figures 1J and S1K). In line

Figure 1. PROX1 Is Expressed in Stem-like Cells in Wnt^{high} CRC Metastases

(A) PROX1 expression in CRC metastases correlates with activated Wnt pathway and stem-like/progenitor signature, and it anticorrelates with differentiation marker KRT20. Correlation analysis is based on GSE41258 (Sheffer et al., 2009). Data are presented as box and whiskers; Spearman correlation coefficient: 1.5 × interquartile range (IQR).

(B) PROX1 expression in CRC metastases correlates with proliferation. Samples from primary tumors and lung metastases (Sheffer et al., 2009) were divided in three categories by PROX1-expression levels. The average expression of proliferation signature (black line) is plotted in $\log_2$ across the six categories. The gray area represents the average expression of all genes.

(C) WNT^{high} CRC stem cells produce higher levels of PROX1. Expression analysis is based on GSE33112 (de Sousa E Melo et al., 2011). Data are presented as box and whiskers; Log expression values: 1.5 × IQR.

(D) PROX1 protein is increased in CRC metastases. Samples were scored as shown in Figure S1C. Student's t test with FDR correction; *$p < 0.05$.

(E) Summary of PROX1 expression analyses in 33 primary tumors and metastases.

(F) PROX1 protein levels correlate with proliferation in CRC metastases. Percentages of PROX1$^+$ and phosphohistone H3$^+$ cells in primary tumors (n = 7) and corresponding lung (n = 10) and liver (n = 6) metastases. Data are presented as mean ± SEM.

(G) PROX1 is expressed in a subset of progenitor/stem cells in CRC metastases. Staining for EPHB2, CD44, BMI1, β-catenin, and phosphohistone H3. Inserts: examples of cytoplasmic and membranous localization of β-catenin. White arrows: cells coexpressing PROX1 and the indicated marker. The scale bar represents 50 μm.

(H and I) Quantification of PROX1 expression data shown in (G). PROX1 expression in the indicated human tumor cell populations (H) or marker expression levels in PROX1$^+$ tumor cells (I). Data are presented as mean ± SEM.

(J) Prox1 is expressed in a subset of mouse transformed intestinal stem/progenitor cells. Staining for Prox1, GFP, EphB2, Krt20, or lysozyme in *Apc$^{fl/fl}$;Lgr5-EGFP-CreERT2* adenomas or normal intestine. Proliferating cells were identified by EdU incorporation assay. The scale bar represents 20 μm.

(K) Prox1 depletion decreases clonogenic growth of AKP organoids. AKP cells were transduced with the control or PROX1 shRNAs, sorted to isolate single GFP$^+$ cells, and plated in Matrigel. Colony number /well was determined at day 15. Student's t test; ***$p < 0.001$. Data are presented as mean ± SEM.

(L) Prox1 mRNA levels in the control or shPROX1 transduced AKP organoids. Student's t test; **$p < 0.01$. Data are presented as mean ± SEM.

(M and N) Stem/progenitor and Wnt target gene expression in AKP organoids following Prox1 depletion at days 5 and 14. Data are presented as mean ± SEM.

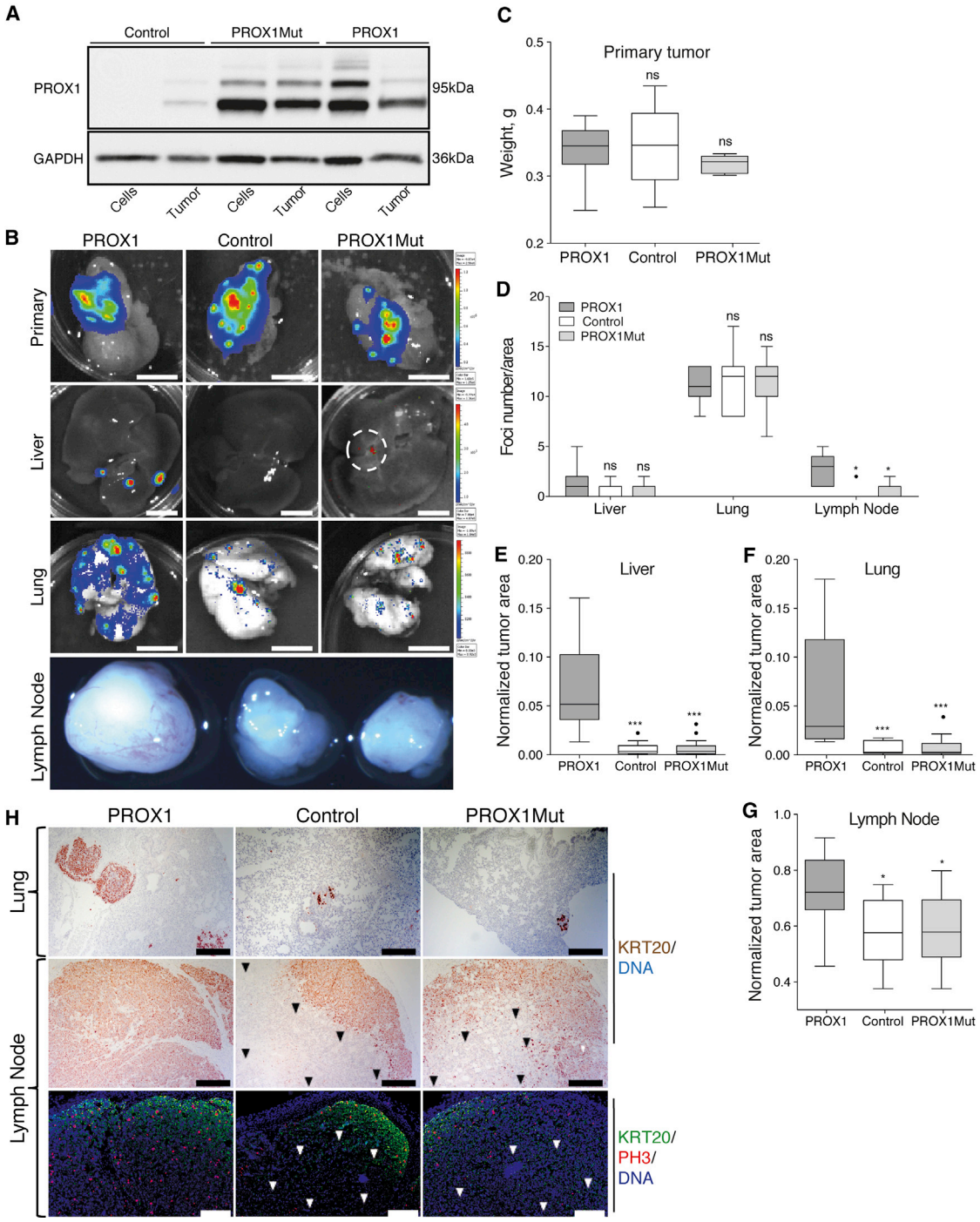

Figure 2. PROX1 Controls CRC Metastasis

(A) PROX1 levels in DLD1-PROX1, DLD1-PROX1mut, or control cells and tumor lysates. Western blotting for the indicated proteins.

(B) PROX1 promotes growth of metastases. Luciferase-tagged DLD1 cells overexpressing wild-type PROX1 (PROX1), mutated PROX1 (PROX1Mut), or transfected with control vector (control) were implanted intracecally in nonobese diabetic (NOD)-severe combined immunodeficiency (SCID); *IL-2Rγ*$^{-/-}$ mice and detected by bioluminescent imaging. The scale bar represents 8 mm.

(C) Comparable size of primary tumors. n = 9/group. Data are presented as box and whiskers; Tukey appearance.

(D) PROX1 overexpression does not affect metastasis incidence. Tumor cells were identified by staining for KRT20. Data are presented as box and whiskers; Tukey appearance.

(E–G) PROX1 promotes growth of individual metastases. One-way ANOVA; *$p < 0.05$; ***$p < 0.001$. Data are presented as box and whiskers; Tukey appearance.

(legend continued on next page)

with previous results, normal intestinal stem cells were Prox1$^-$ (Petrova et al., 2008; Figures 1J and S1L). These data show that, as in human tissues, a subset of transformed intestinal stem cells produces high levels of Prox1. Furthermore, a proportion of GFP^{low}/EphB2$^+$/EdU$^+$ adenoma progenitor cell population, but not more-differentiated cells, maintain Prox1 expression. We conclude that (1) PROX1 expression partially overlaps with other cancer stem cell (CSC)/progenitor markers, (2) many proliferating cells in the tumors are PROX1-negative, (3) PROX1 is not expressed in differentiated cells, and (4) PROX1 expression is increased in metastases in comparison to the primary tumors. Thus, PROX1 is induced only upon transformation and it defines a subset of cancer stem/progenitor cells, which themselves are moderately proliferative but, when present in metastases, signify high proliferative activity.

PROX1 Controls CSC Colony-Forming Ability

To study whether PROX1 contributes to the clonogenic growth of CRC cells, we used intestinal organoids from *Apc*$^{fl/fl}$; *Kras*$^{Lsl\text{-}G12D}$; *Tp53*$^{fl/fl}$;*villin-CreERT2* (*AKP*) mice. In addition to high Wnt signaling, such intestinal epithelial cells carry an oncogenic mutation in *Kras* and loss of the tumor suppressor p53, thus recapitulating major pathways important for development of CRC (Fearon, 2011). Similar to human CRCs and *Apc*$^{fl/fl}$; *Lgr5-EGFP-Ires-CreERT2* adenomas, we observed partially overlapping localization of Prox1 and intestinal stem cell/progenitor markers Lgr5, nuclear β-catenin, EphB2, and Cd44; proliferation markers phosphohistone H3 and Ki67; and absence of Prox1 expression in differentiated Krt20$^+$ and Krt6$^+$ cells (Figures S1M and S1N). We next tested whether Prox1 is necessary to sustain growth of AKP organoids in a colony-forming assay, where a single stem cell gives rise to a 3D "organoid" structure (Sato et al., 2011). Downregulation of Prox1 significantly decreased the number of colonies formed by single AKP cells, thus demonstrating that Prox1 maintains clonogenic growth (Figures 1K and 1L). Expression of progenitor/stem cell markers and Wnt target genes Lgr5, Ascl2, Rnf43, and EphB2 was not modified in early organoids at day 5, despite downregulation of Prox1 (Figure 1M). However, their expression was lower in organoids by day 15 (Figure 1N). Taken together with our previous data showing that Prox1 does not affect general Wnt reporter activity (Petrova et al., 2008), these results indicate that Prox1 does not directly regulate stem/progenitor gene expression or general Wnt signaling, but it rather maintains the clonogenic capacity of CSCs.

PROX1 Controls CRC Metastasis

Analyses of human tumor samples indicated that PROX1 expression is elevated in a subset of metastases (Figure 1E), consistent with potential involvement of PROX1 in metastatic CRC. To clarify this, we used an orthotopic model, in which CRC cells form metastases in lymph nodes, liver, and lungs after intracecal injection (Céspedes et al., 2007). To study if PROX1 is sufficient to promote metastasis, we overexpressed PROX1 and its inactive form PROX1mut, bearing mutations in the DNA-binding domain, in PROX1-negative DLD1 CRC cells. As another control, we used cells transfected with an empty vector (Figure 2A). The primary tumor size was similar between the groups, and there was no difference in primary tumor weights (Figures 2B and 2C). However, significantly more DLD1-PROX1 cells were present in lungs, liver, and lymph nodes (Figure 2B). Metastatic incidence was increased only in lymph nodes of PROX1 group (Figure 2D). In all tissues, PROX1$^+$ metastases were 2- to 5-fold larger than the control lesions (Figures 2E–2G). PROX1$^+$ metastases displayed higher levels of proliferation marker phosphohistone H3. Strikingly, proliferating cells were observed throughout the lesion in DLD1-PROX1 metastases, whereas in the control, metastases proliferation was restricted to the outer rim as a result of massive central necrosis (Figure 2H).

We next asked whether PROX1 depletion in PROX1$^+$ SW620 cells affects development of metastases (Figures S2A–S2C). Depletion of PROX1 did not affect growth of primary tumors; however, we observed marked differences in the development of metastases (Figures S2D–S2F). In this case, there were more PROX1$^+$ metastases, which were also bigger in comparison to the controls (Figures S2E and S2F). Depletion of PROX1 reduced metastases proliferation and induced extensive necrosis and apoptosis, whereas little cell death was observed in primary tumors (Figures S2G and S2H).

To confirm that these phenotypes were not the result of long-term cell selection, we studied SW480R/PROX1si cells, in which PROX1 is suppressed upon administration of doxycycline (Petrova et al., 2008; Figure S2I). Depletion of PROX1 reduced metastases size and incidence without affecting the primary tumor (Figures S2J and S2K). Doxycycline treatment had no effect on SW480R/GFPsi metastases, in which a control small hairpin RNA (shRNA) was induced (Figures S2J and S2L). Similar to other models, suppression of PROX1 resulted in formation of large central necrotic areas (Figure S2M). In summary, loss- and gain-of-function experiments show that PROX1 is necessary and sufficient to promote CRC metastases.

PROX1 Fuels Metastases Outgrowth

Metastasis requires several steps: invasion, extravasation, survival in the circulation, colonization of distal organs, and outgrowth of macrometastases (Chaffer and Weinberg, 2011). PROX1 promoted EMT in vitro by suppressing E-cadherin (Lu et al., 2012). However, in our hands, PROX1$^-$ and PROX1$^+$ cells expressed comparable levels of E-cadherin and EMT marker vimentin (Figures 3A and S3A). PROX1 did not increase invasion in in vitro assays or local invasion in primary tumors, and vascular density was comparable in PROX1$^+$ versus PROX1$^-$ tumors (Figures S3B–S3E). Thus, enhanced local invasion and angiogenesis are not major contributing factors in our models.

To test the role of PROX1 during the subsequent steps of metastasis, we injected enhanced GFP (EGFP)-tagged SW620

(H) Only wild-type PROX1 promotes growth of metastases. Upper row: increased size of DLD1-PROX1 lung metastases. Middle row: decreased cell death in DLD1-PROX1 metastases. Arrows, necrotic areas. Lower row: increased proliferation in DLD1-PROX1 metastases. Chromogenic staining for KRT20 (brown) or fluorescent staining for phosphohistone H3 (red), KRT20 (green), and DNA (blue). The scale bars represent 200 μm (upper and middle panels) and 100 μm (lower panel).

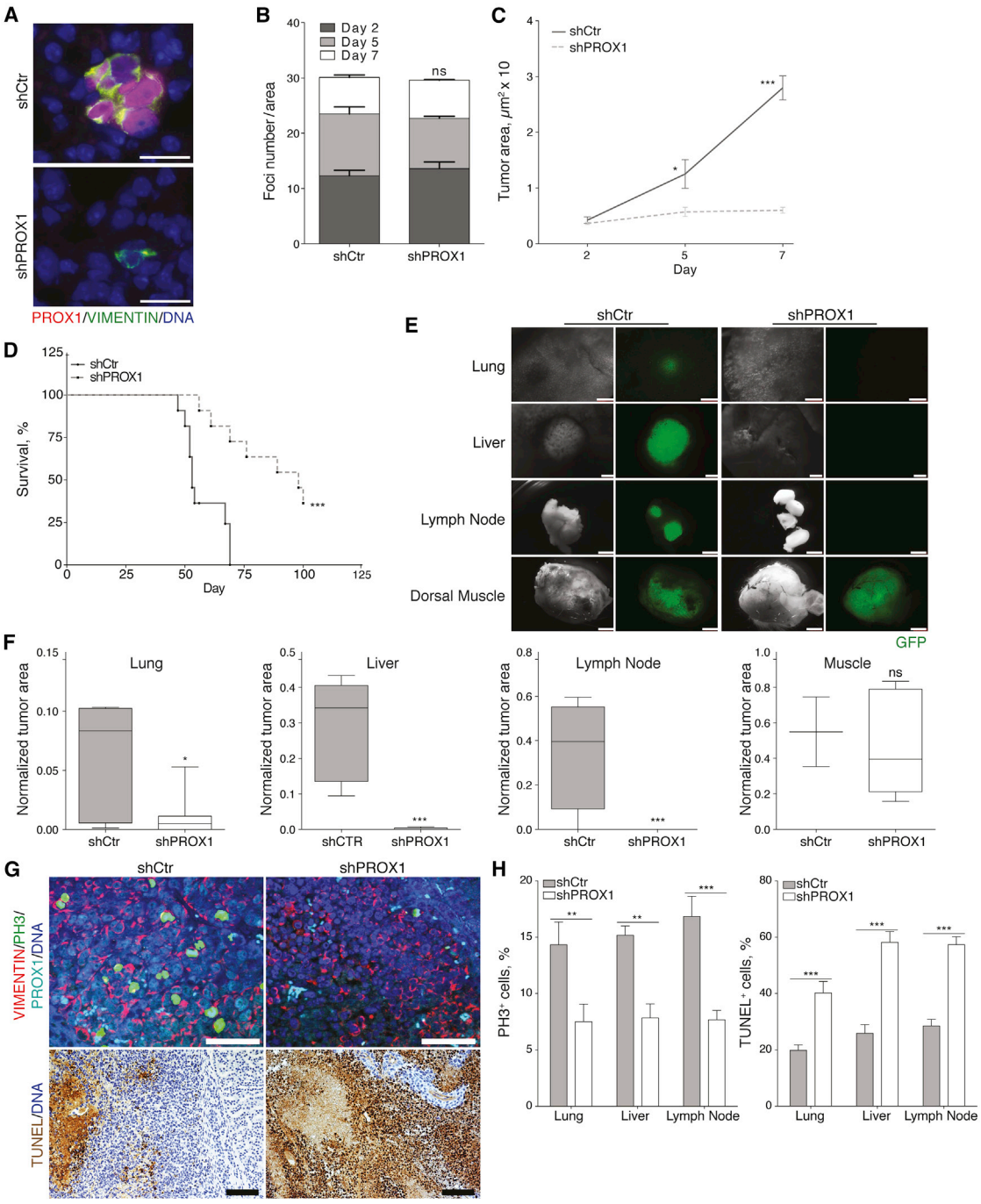

Figure 3. PROX1 Promotes Metastatic Outgrowth

(A) Lung micrometastases 3 days after the tail vein injection of SW620-shCtr or SW620-shPROX1 cells. Staining for PROX1 (red), vimentin (green), and DNA (blue). The scale bar represents 20 μm.

(B) PROX1 is dispensable for tumor cell extravasation. Number of lung metastatic foci after injection of SW620-shCtr or SW620-shPROX1cells into the tail vein of NOD-SCID; *IL-2Rγ*$^{-/-}$ mice. Tumor cells were stained for human vimentin. Data are presented as mean ± SEM.

(C) PROX1 promotes growth of metastases. Average size was calculated by dividing total metastases area by number of metastases and normalized to tissue area analyzed. Two-way ANOVA; *p < 0.05; ***p < 0.001. Data are presented as mean ± SEM.

(D) PROX1 depletion prolongs survival. Kaplan-Meyer survival curve of mice injected with SW620-shCtr or SW620-shPROX1 cells. Log rank (Mantel-Cox) test; ***p < 0.001.

(E) PROX1 depletion prevents growth of macrometastases. Ex vivo analysis of SW620-shCtr and SW620shPROX1 EGFP^{+} cells 7 weeks after tail vein injection into NOD-SCID; *IL-2Rγ*$^{-/-}$ mice. The scale bars represent 750 μm (lung), 1 mm (liver), and 2.5 mm (lymph node and dorsal muscle).

(legend continued on next page)

PROX1$^+$ and PROX1$^-$ cells into the tail vein. PROX1$^+$ or PROX1$^-$ CRC cells formed similar number of lung colonies at days 2, 5, and 7 post-injection (Figures 3A and 3B). Thus, PROX1 is dispensable for tumor cell survival in the blood stream or in early metastases. However, PROX1 depletion prevented further metastatic outgrowth and increased animal survival (Figures 3C and 3D). PROX1$^-$ cells were unable to establish colonies in most organs, with a notable exception of skeletal muscle (Figures 3E and 3F). Similar to orthotopic models, proliferation and apoptosis were increased and decreased, respectively, in PROX1$^+$ metastases compared to PROX1$^-$ lesions, as determined by phosphohistone H3 staining and TUNEL assay (Figures 3G and 3H). Overall, these results indicate that PROX1 mainly promotes outgrowth of tumor cells in target organs.

PROX1 Promotes Resistance to Hypoxia and Nutrient Deprivation

To investigate the underlying mechanism of PROX1-mediated metastatic outgrowth, we analyzed cell growth under standard cell culture conditions. Modulation of PROX1 levels in three human CRC lines did not affect cell growth in 2D (Figures 4A and S4A). We next studied the ability of these cells to form tumor spheroids. In agreement with *AKP* organoid results, in all three lines, PROX1$^+$ spheroid size and number were increased in comparison to PROX1-negative spheroids (Figures 4B–4E and S4B–S4D). Consistent with in vivo models, PROX1$^+$ spheroids proliferated more and underwent apoptosis less than PROX1$^-$ spheroids (Figures 4F–4I and S4D).

In tumor spheroids, diffusion of nutrients and oxygen is decreased in the center, resulting in a hypoxic/low-nutrient environment and cell death (Hirschhaeuser et al., 2010). Whereas the central part of PROX1$^-$ spheroids was filled with dead cells, PROX1$^+$ spheroids cores contained live cells and more cells proliferated at a distance from the surface (Figure 4J), suggesting that PROX1 promotes cell survival and proliferation in hypoxia and nutrient-poor environments. To directly test this, we cultured DLD1-PROX1 and DLD1 control cells in 0.1% O_2 and/or under reduced glucose or glutamine conditions. Hypoxia induced stabilization of HIF1α in both PROX1$^-$ and PROX1$^+$ DLD1 cells (Figures 5A and 5B). However, by 72 hr, DLD1 control cells became growth arrested and apoptotic, as determined by staining for activated caspase-3 (Figures 5C–5F). In contrast, hypoxic DLD1-PROX1 cells had somewhat enhanced proliferation and low cell death (Figures 5D, 5F, and 5G). PROX1$^+$ cells were also more resistant to cell growth arrest and cell death elicited by the low glucose or glutamine, but not by etoposide, which induces apoptosis through DNA damage (Figures 5D, 5F, 5G, and S5A). Similar results were observed in another cell line SW620 (Figures S5A–S5D). These data indicate that PROX1 sustains cell survival and proliferation under metabolic stress.

PROX1 Promotes Metabolic Adaptation

Increased glycolysis is one of the key characteristics of cancer cells. However, cancer cells can also use oxidative phosphorylation rather than glycolysis to sustain growth (e.g., Haq et al., 2013; Janiszewska et al., 2012). To better understand the mechanisms of increased fitness of PROX1$^+$ CRC cells, we studied their metabolic responses upon nutrients or oxygen deprivation. Extracellular acidification rate (ECAR), a measure of glycolysis, and cellular oxygen consumption rate (OCR), a measure of oxidative phosphorylation, were comparable between DLD1-PROX1$^+$ and PROX1$^-$ cells under basal cell culture conditions (Figures 5H and 5I). As expected, glucose deprivation decreased glycolysis in both cells types (Figure 5H). PROX1$^-$ cells displayed little compensatory increase in OCR, indicative of their inability to switch to an alternative fuel source. In contrast, OCR was high in PROX1$^+$ cells upon glucose deprivation, which also paralleled increased survival of PROX1$^+$ cells (Figures 5I and 5G). In the absence of glutamine, PROX1$^+$ cells, unlike the control cells, sustained both OCR and ECAR and increased glycolysis after treatment with the mitochondrial oxidative phosphorylation inhibitor trifluorocarbonylcyanide phenylhydrazone (Figures S5E and S5F). Better adaptation to glucose or glutamine starvation and oxidative phosphorylation inhibition was also observed in PROX1$^+$ SW620 cells (data not shown).

In order to evaluate cell metabolism in hypoxia, we measured ECAR and OCR in cells cultured for 24 hr in 0.1% O_2. SW620 PROX1$^+$ cells had higher basal level of oxidative phosphorylation in normoxia and also displayed a higher glycolysis rate in response to hypoxia (Figures S5G and S5H). Similarly, DLD1-PROX1 cells cultured in hypoxia and low glutamine displayed higher levels of glycolysis in comparison to the control cells (data not shown). Taken together, these data indicate that, whereas not favoring either oxidative phosphorylation or glycolysis, PROX1 promotes cell adaption to changes in fuel source. Such metabolic fitness of PROX1$^+$ cells would confer growth advantages under unfavorable conditions that tumor cells encounter during metastasis outgrowth.

Continuous PROX1 Expression Is Necessary for Growth CRC Metastases

To evaluate the therapeutic potential of targeting PROX1, we studied whether ablation of PROX1 affects established metastases. SW480R/PROX1si cells, expressing a PROX1-targeting shRNA under the control of doxycycline, were injected intracecally. Doxycycline treatment was initiated 30 days later, when both primary and metastatic lesions already developed. PROX1 depletion did not affect primary tumors, despite downregulation of PROX1 protein (Figures 6A, 6B, and S6A). However, further growth of metastases was arrested in the absence of PROX1, whereas they continued to grow in the control mice (Figures 6A, 6C, S6B, and S6C). Thus, PROX1 inhibition may be a

(F) Quantification of macrometastases size. Student's t test; *$p < 0.05$; ***$p < 0.001$. Data are presented as box and whiskers; Tukey appearance.
(G) Increased proliferation (upper row) and decreased necrosis (lower row) in SW620shCtr liver metastasis. Staining for human vimentin (red), phosphohistone H3 (green), and DNA (blue) or chromogenic TUNEL assay (brown). The scale bars represent 50 μm (upper) and 100 μm (lower).
(H) Quantification of cell proliferation or apoptosis in metastases. Proliferating cells were determined by staining for phosphohistone H3 and apoptosis by TUNEL assay. Two-way ANOVA; **$p < 0.01$; ***$p < 0.001$. Data are presented as mean ± SEM.

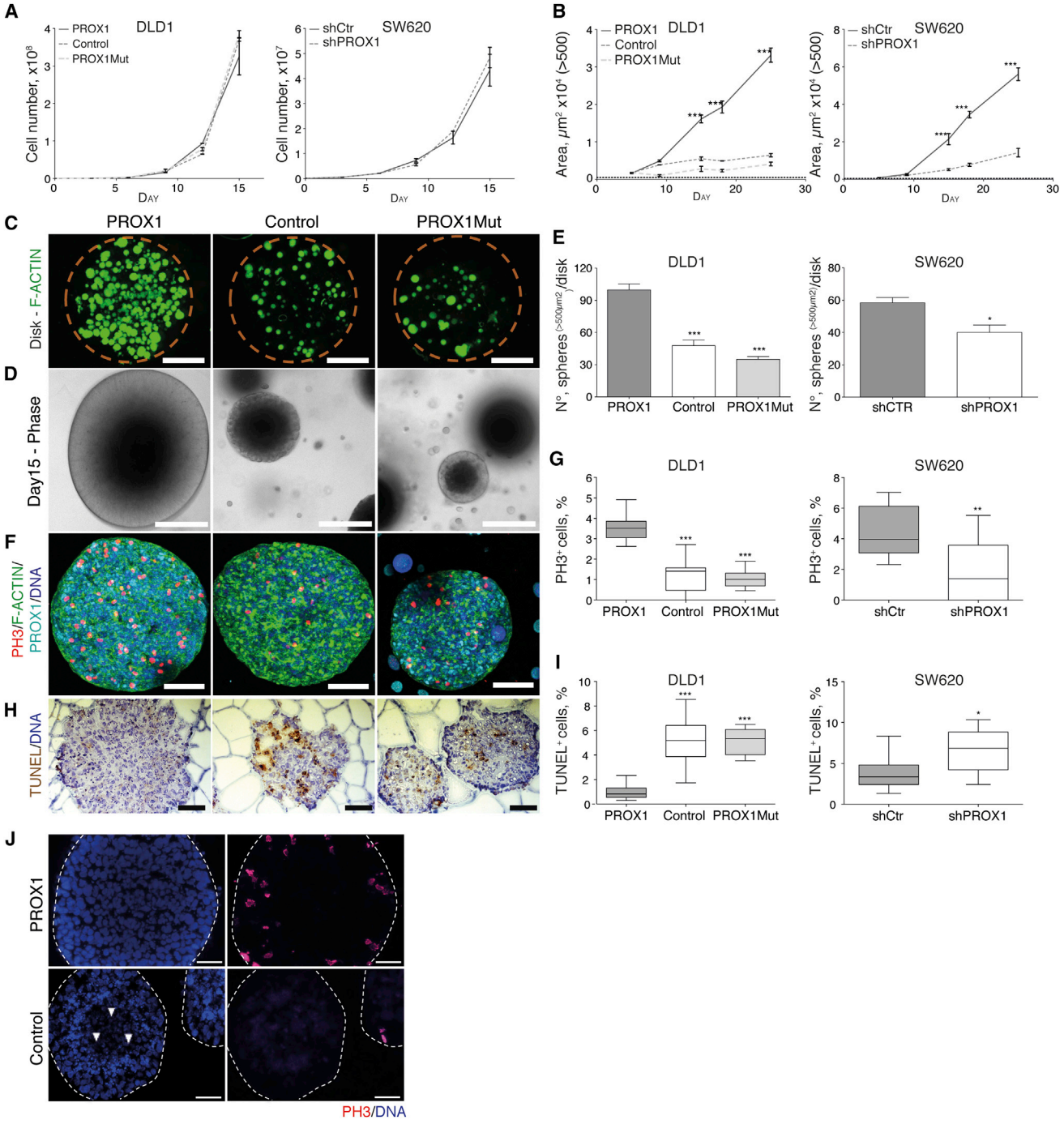

Figure 4. PROX1 Promotes Cell Growth and Survival in 3D

(A) PROX1 does not affect cell growth in 2D conditions. Growth curves of DLD1 PROX1 control or PROX1Mut and SW620 shCtr or shPROX1 cells. Two-way ANOVA; not significant (ns). Data are presented as mean ± SEM.

(B) PROX1 promotes growth of tumor spheroids. Cells seeded in qGel were cultured in complete culture medium and spheroid size determined by phase-contrast microscopy. Threshold >500 μm^2 was used. Two-way ANOVA; ***$p < 0.001$. Data are presented as mean ± SEM.

(C) Macroscopic view of tumor spheroids. Cells were stained for F-actin (green) 21 days after seeding. The scale bar represents 2.5 mm.

(D) Microscopic appearance of PROX1, control, or PROX1Mut spheroids at day 15. The scale bar represents 200 μm.

(E) Quantification of spheroids number at day 21. Data are presented as mean ± SEM.

(F) PROX1 promotes proliferation of spheroids. Whole-mount staining for phosphohistone H3 (red), F-actin (green), PROX1 (light blue), and DNA (dark blue). The scale bar represents 100 μm.

(legend continued on next page)

useful therapeutic option for treatment of PROX1$^+$ CRC metastases.

Pharmacological Inhibition of Autophagy Targets Metastatic PROX1$^+$ Cells

With few exceptions, therapeutic targeting of transcription factors is difficult (Koehler, 2010). Therefore, we sought to identify pharmacological approaches for targeting PROX1$^+$ CRC cells. One of the pathways that mediate stress-induced metabolic adaptation is autophagy, a process of recycling cell components to maintain nutrient flux and energy homeostasis (White, 2012). To test whether autophagy underlies PROX1-induced survival under metabolic stress, we treated cells with chloroquine (CQ), which inhibits autophagy by preventing endosomal acidification. CQ-treated PROX1$^+$ and PROX1$^-$ cells accumulated enlarged LC3B$^+$ autophagosomes in hypoxia, demonstrating efficient autophagy inhibition (Figure S6D). CQ prevented proliferation of hypoxic PROX1$^+$ cells, whereas it had little effect on PROX1$^+$ or PROX1$^-$ cells under normoxic conditions (Figures 6D, 6E, and S5E). We also treated cells with another autophagy inhibitor, 3-methyl adenine (3-MA) (White, 2012). Similar to the CQ, 3-MA induced cell death of PROX1$^+$ cells under hypoxic conditions (Figure S6F). Thus, autophagy inhibition and metabolic stress induce a synthetically lethal phenotype in PROX1$^+$ cells. It also suggests that autophagy inhibition, which is now under clinical trials in metastatic CRC (http://clinicaltrials.gov/show/NCT01006369), may preferentially target PROX1$^+$ tumor cells.

To evaluate this hypothesis, we injected mice intravenously with PROX1$^+$ or PROX1$^-$ SW620 cells and monitored the effects of CQ on liver metastases. CQ was administered either at high (40 mg/kg; Sasaki et al., 2012) or at low (10 mg/kg) dosage, which better mimics the situation in patients (Kimura et al., 2013). The high-CQ regimen significantly reduced the size, but not the number, of liver metastases (Figures S6G and S6H). Strikingly, these macrometastases had increased necrosis, with frequently only a rim of live cells (Figures S6I and S6J). PROX1$^-$ cells did not form liver macrometastases at this time point, and CQ had no further effect on cell death (Figures S6G–S6I). Importantly, although low-CQ regimen did not reduce liver macrometastasis incidence or size (Figures 6F and S6K), it still strongly induced tumor necrosis and decreased cell proliferation (Figures 6G, 6H, S6L, and S6M).

Decreased angiogenesis can also lead to tumor necrosis. Therefore, we quantified tumor vessel density. Vascular density was comparable in treated versus control metastases (Figures 6H and S6N), arguing that CQ acts directly on tumor cells. Proliferating cells in CQ-treated tumors were found only at the tumor-stroma interface, characterized by abundant vasculature, showing that treated cells need oxygen- and nutrient-replete conditions to proliferate (Figures 6H, S6L, and S6N).

Intriguingly, PROX1 had little effect on orthotopically implanted primary tumors, whereas it promoted growth of metastases (Figures 2, 6A–6C, and S2). To explain this differential response, we analyzed proliferation and apoptosis in metastases versus primary tumors. In two different models, PROX1$^+$ and PROX1$^-$ primary tumors proliferated at low and comparable rates and had low levels apoptosis (Figures 6I, 6J, and S6O; data not shown). In contrast, proliferation was high in PROX1$^+$ metastases, whereas apoptosis was induced in PROX1$^-$ metastases (Figures 6J and S6O). Because only PROX1$^+$ cells can productively use autophagy (Figure 6D), we compared responses to autophagy inhibition of primary tumors and metastases. Treatment with CQ did not affect primary tumor proliferation (Figures 6K, 6L, and S6P) or metastasis incidence (Figure S6Q). However, CQ significantly suppressed proliferation of PROX1$^+$ metastases (Figures 6K and 6L). Furthermore, although CQ treatment did induce some necrosis in primary tumors, necrosis levels were significantly higher in PROX1$^+$ metastases (Figure 6M). Importantly, the treatment had no effect on vascular density (Figure S6R).

To better understand why PROX1$^+$ metastases respond better than primary tumors to autophagy inhibition, we next compared autophagy in primary versus metastatic lesions by quantifying differences in LC3B levels between the control and CQ-treated lesions. Such autophagic flux is a more accurate measure of autophagy than the steady-state level of processed LC3B (Mizushima et al., 2010). Autophagic flux was higher in metastases, regardless of the levels of PROX1 (Figures 6N–6Q). Our data thus show that CQ efficiently targets PROX1$^+$ cells in macrometastases. They also indicate that the metastatic CRC cells have higher levels of autophagy, which points to increased metabolic stress in the sites of metastases. Although the mechanisms remain to be elucidated, these results show that PROX1$^+$ metastases may respond to autophagy inhibition in patients.

BCL2L15 Is a Direct Target of PROX1, which Suppresses Tumor Growth

To study the transcriptional network regulated by PROX1, we carried out chromatin immunoprecipitation sequencing (ChIP-seq) and transcriptome analysis after small interfering RNA (siRNA)-mediated knockdown of PROX1 in SW480R cells (Figure S7A). The analyses identified 23,450 PROX1-binding sites (false discovery rate [FDR] < 0.001) and 444 PROX1-dependent genes (FDR < 0.05 and fold change [FC] > 1.5). To find how PROX1 DNA binding correlates with changes in gene expression, we mapped these genes to nearby ChIP-seq-binding regions. Unaffected genes (mean expression value >8 and FC < 1.5) were used as reference. We observed that PROX1 preferentially binds in the vicinity of genes induced by PROX1 depletion (Figure S7B). Thus, as found in other cell types (e.g., Steffensen et al., 2004), PROX1 acts as a transcriptional repressor.

(G) Quantification of proliferation in tumor spheroids. Data are presented as box and whiskers; Tukey appearance.
(H) Decreased apoptosis in PROX1-expressing spheroids. Staining for TUNEL assay (brown) and DNA (light blue). The scale bar represents 100 μm.
(I) Quantification of apoptosis, shown as percentage TUNEL$^+$ cells in sections. DLD1, one-way ANOVA; ***$p < 0.001$. SW620, Student's t test; ***$p < 0.001$. *$p < 0.05$; **$p < 0.01$. Data are presented as box and whiskers; Tukey appearance.
(J) Necrotic core is present in control but PROX1-expressing spheroids. Staining for PH3 (red) and DNA (blue). White arrowheads, necrotic areas. The scale bar represents 50 μm.

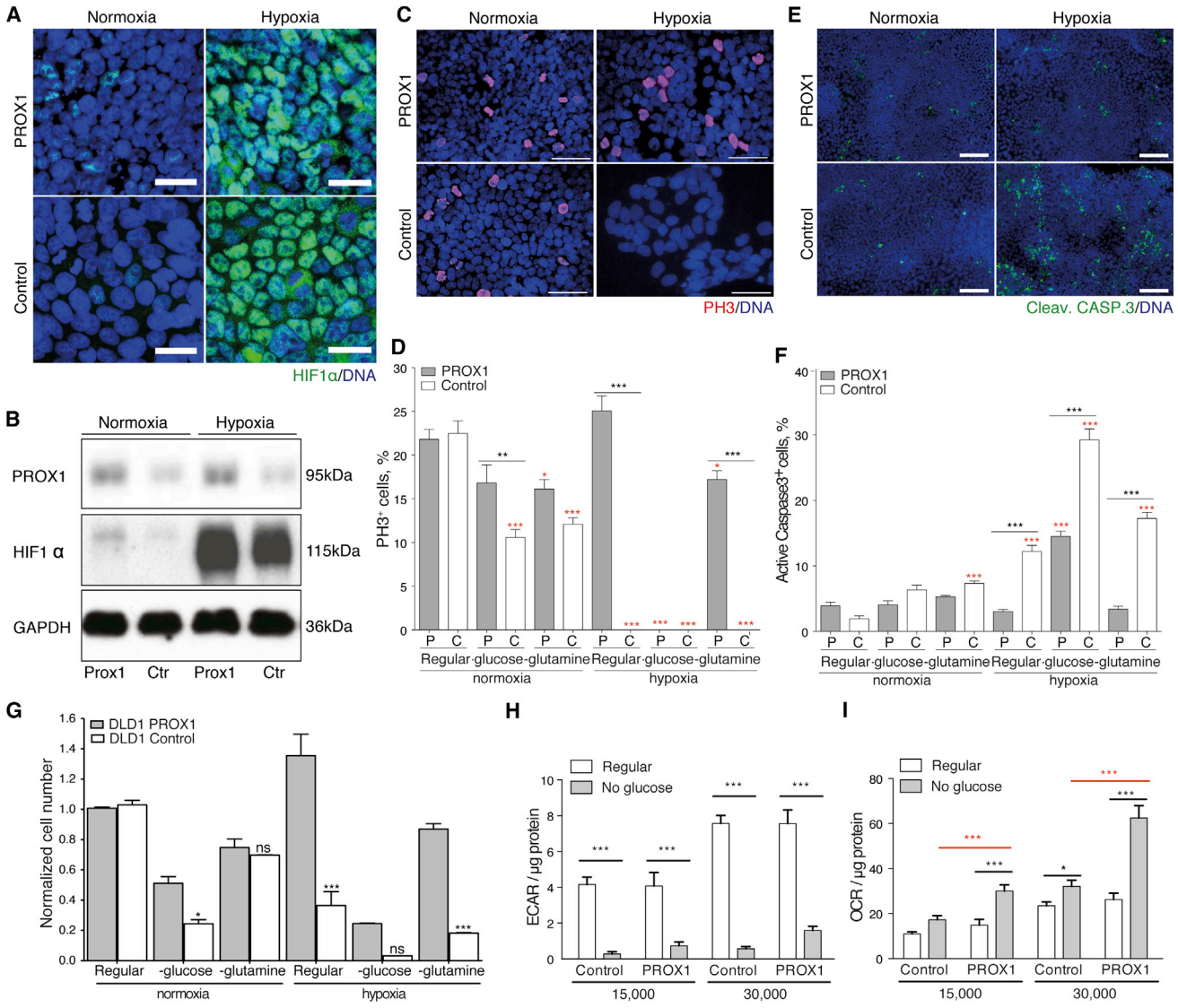

Figure 5. PROX1 Promotes Metabolic Adaptation In Vitro

(A) HIF1α is stabilized by hypoxia both in DLD1-PROX1 or control cells. Staining for HIF1α (green) and DNA (blue). The scale bar represents 50 μm.

(B) HIF1α levels in PROX1$^+$ or PROX1$^-$ cells after 12 hr in hypoxia. Western blotting for the indicated proteins.

(C) PROX1$^+$ cells proliferate in hypoxia. Cells were cultured in normoxia or 0.1% O_2 for 72 hr. Staining for PH3 (red) and DNA (blue). The scale bar represents 50 μm.

(D) PROX1$^+$ cells proliferate under metabolic stress. Cells were cultured in the indicated conditions for 72 hr and stained for phosphohistone H3 and DNA. Data are presented as mean ± SEM.

(E) PROX1 reduces cell apoptosis under metabolic stress conditions. Staining for cleaved caspase-3 (green) and DNA (blue) after 72 hr. The scale bar represents 200 μm.

(F) Quantification of apoptosis for data shown in (E). One-way ANOVA; $^{**}p < 0.01$; $^{***}p < 0.001$. Black *, PROX1 versus control. Two-way ANOVA; $^*p < 0.05$; $^{***}p < 0.001$. Red *, treatment versus complete medium in normoxia. Data are presented as mean ± SEM.

(G) Quantification of DLD1 cell number after 3 days incubation in the indicated conditions. $^*p < 0.05$; $^{***}p < 0.001$. Cell number was determined by CyQuant assay. Data are presented as mean ± SEM.

(H) Glucose deprivation decreases lactate production in both DLD1-PROX1 and control cells. ECAR was measured in cells cultured at two different densities. Data are presented as mean ± SEM.

(I) PROX1$^+$, but not control, cells increase oxidative phosphorylation in the absence of glucose. OCR was measured in the same samples as for (H). Data are presented as mean ± SEM. Two-way ANOVA; $^*p < 0.05$; $^{**}p < 0.005$; $^{***}p < 0.001$; red *, PROX1 versus control in indicated condition; black *, significant change of the same cell type in different conditions.

As PROX1 promoted survival of both DLD1 and SW480R cells, we reasoned that important direct targets should be repressed in both cell lines. To identify such targets, we combined ChIP-seq data with gene expression profiling results in two cell types. We identified 40 genes, repressed by PROX1 and carrying PROX1-binding sites (FDR < 0.05; Tables S1, S2, and S3), out of which seven genes (*ABAT*, *BCL2L15*, *CAV1*, *IQGAP2*, *SEMA3C*, *SLC7A7*, and *TNFRSF9*) were repressed by PROX1 more than 2-fold (Figures 7A, S7C, and S7D). For most of these genes, the direct connection to CRC progression remains to be investigated. However, BCL2 family member, BCL2L15, acts as a conditional pro-apoptotic gene in CRC cells in vitro (Dempsey et al., 2005) and *Cav1*$^{-/-}$ mice have more aggressive lesions in a genetic model of intestinal cancer (Friedrich et al., 2013).

We tested next whether metabolic stress conditions affected the expression of BCL2L15 and CAV1. Hypoxia induced expression of BCL2L15 and CAV1 in PROX1^{-}, but not PROX1^{+} cells, suggesting that they act as PROX1 effectors in cells under metabolic stress (Figures 7B and 7C). At the same time, PROX1^{+} and PROX1^{-} cell response to hypoxia was comparable, as judged by expression levels of the HIF1α target VEGF-A (Figure 7D). We overexpressed BCL2L15, CAV1, or another PROX1 target TNFRSF9 in PROX1^{+} CRC cells (Figure S7E) and tested growth and survival of these cells under normoxia and hypoxia. BCL2L15 and, to a lesser extent, CAV1 reduced proliferation and increased apoptosis of PROX1^{+} cells under hypoxia (Figures 7E, 7F, and S7F). In contrast, overexpression of TNFRSF9 had no effect (Figure S7F). Furthermore, BCL2L15 overexpression in PROX1^{+} CRC cells drastically reduced the number and size of metastases after intravenous (i.v.) injections (Figures 7G–7J). To test the effects of BCL2L15 inactivation, we used the *AKP* intestinal organoid model, in which Bcl2l15 is expressed in Prox1-negative cells and is further induced after Prox1 depletion (Figures S7G and S7H). We found that Bcl2l15 depletion enhanced clonogenic growth of intestinal organoids in vitro (Figures 7K and S7I), as well as proliferation and growth of organoid-derived tumors in vivo (Figures 7L–7N and S7J), without affecting cell survival (Figure 7O). As expected, Prox1 depletion reduced colony formation and tumor growth under the same conditions (Figures 7K–7O, S7I, and S7J).

To further analyze the significance of BCL2L15 and CAV1 regulation by PROX1 in human CRC in vivo, we studied BCL2L15 and CAV1 protein localization in human CRC. BCL2L15 and PROX1 displayed a mutually exclusive localization pattern both in metastases and primary tumors (Figures 7P and S7K; data not shown). In contrast, CAV1 was generally low in CRC cells independently of PROX1 status (data not shown). These results suggest that BCL2L15 suppression is a more-specific marker for PROX1 activity. Moreover, luciferase reporter assays showed that PROX1 directly repressed the activity of the 3′ PROX1-binding region in the BCL2L15 locus (Figures S7L and S7M). BCL2L15 mRNA levels were also strongly reduced in CRC tumors ($n = 230$; $p = 2.11 \times 10^{-8}$; Figure 7Q) and showed a significant negative correlation with PROX1 (Figure 7Q; $p = 1.8 \times 10^{-4}$). In summary, our genome-wide analyses identified a number of potential direct PROX1 targets in CRC (Table S1), whose roles still need to be investigated. Here, we show that BCL2L15 is an important, even if likely not the only, effector of PROX1 in CRC, whose suppression in part recapitulates the effects of PROX1.

DISCUSSION

We report that the colon-cancer-specific Wnt target PROX1 is highly expressed in colon cancer metastases, where it is present in a subset of cancer stem/progenitor cells. We also show that, in advanced CRC, PROX1 sustains growth of macrometastases through the evasion of apoptosis and metabolic adaptation. Previous studies investigated the mechanisms of local invasion in primary CRC tumors. They established important roles for Wnt and Notch signaling, EMT, and the tumor-stroma interactions (e.g., Dolznig et al., 2011; Sonoshita et al., 2011; Spaderna et al., 2008; Wolf et al., 2012). However, mechanisms governing outgrowth of metastases are not well understood. Yet metastatic CRC is a major clinical challenge, with limited patient survival and few therapeutic options available, especially for patients with activating KRAS mutations, which confer resistance to anti-EGFR therapy (Cunningham et al., 2010; Van Emburgh et al., 2014).

In this study, we investigated the role of the transcription factor PROX1 in the development of CRC metastases. Expression of PROX1 in primary CRC tumors is not an independent prognostic factor (Skog et al., 2011). However, we found that PROX1 levels are generally increased in metastases and a proportion of PROX1^{-} primary tumors give rise to PROX1^{+} metastases. Large expression data sets from metastatic lesions will clarify whether high levels of expression of PROX1 in a metastasis correlates with survival after relapse. Nevertheless, already now our data suggest that, in advanced CRC, PROX1 may be important in the context of metastatic disease.

Analysis of PROX1 expression patterns in human metastases and mouse models demonstrated that PROX1 is expressed only upon transformation and it may delineate a distinct subpopulation of cancer stem/progenitor cells. Furthermore, in vitro analyses of the intestinal organoid model demonstrated that, while Prox1 does not directly control the expression of stem/progenitor-associated genes or general Wnt pathway activity, it is essential to maintain clonogenic growth. Our data are in agreement with the results of Wiener et al., who show that Prox1 is essential for the expansion of the stem cell pool in transformed but not in normal intestinal stem cells (Wiener et al., 2014). Through the analysis of mouse models of CRC metastasis, we found that PROX1 is dispensable for growth of primary tumors, cell survival in the bloodstream, or extravasation; however, it promotes outgrowth of metastases. At least in part, this property of PROX1 relies on its ability to override cell death imposed by metabolic stress, such as hypoxia or low-nutrient environment. Taken together, our data suggest that, in CRC metastases, there exists a subpopulation of PROX1^{+} stem/progenitor cells, which are highly resistant to metabolic insults and can thus fuel metastatic growth. These data identify PROX1 as an important player in CRC stem/progenitor cells maintenance and function.

To investigate the mechanisms of PROX1 action in CRC, we carried out PROX1 genome location analysis and identified genes regulated by PROX1. As expected, a significant number of direct PROX1 target genes were identified (Table S1), and

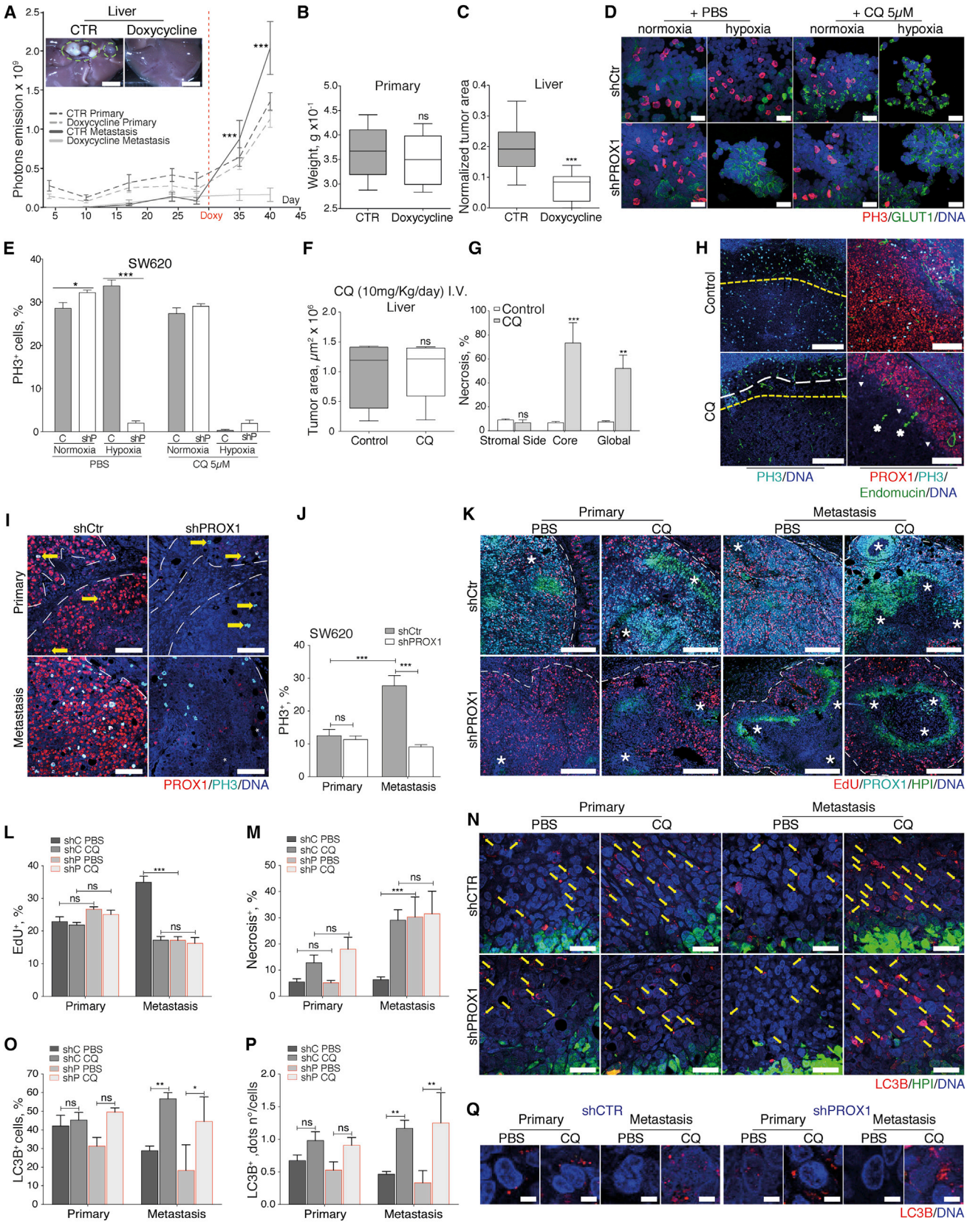

(legend on next page)

we began investigating their individual contribution. Here, we show that a pro-apoptotic member of the BCL2 family, BCL2L15 (Dempsey et al., 2005), is induced in hypoxic PROX1^{-}, but not PROX1^{+}, cancer cells and that BCL2L15 can in part recapitulate the phenotype of PROX1 deficiency, such as increased clonogenic growth of tumor organoids or tumor development in vivo. These results indicate that apoptosis evasion under metabolic stress conditions is important for the prosurvival function of PROX1^{+} in metastases. Most likely, the role of other potentially interesting targets and their combinatorial interactions will need to be addressed in the future. Of interest, Annexin A1, identified as a PROX1 effector by Wiener et al. (2014) is another direct target of PROX1 in our data set (Table S1).

With few exceptions, transcription factors are considered undruggable. To overcome this limitation, we searched for pharmacological approaches to target PROX1^{+} tumor cells. We found that inhibition of autophagy, a catabolic process providing an alternative energy source, eliminates the growth advantage of PROX1^{+} CRC cells and decreases metastatic burden. Of interest, following CQ treatment, viable tumor cells are located in the vicinity of blood vessels and they remain accessible for cytotoxic drugs. Thus, a combination of targeted anti-PROX1 therapy with antiproliferative/cytotoxic 5-fluorouracil-based chemotherapy might be pursued as a potential treatment option for CRC patients with PROX1^{+} metastatic disease.

We propose the following working model of PROX1's role in metastasis: high Wnt signaling induces PROX1 expression in CRC cells and PROX1^{+} cancer stem/progenitor cells become resistant to metabolic stress, in part through the repression of BCL2L15. Because PROX1 is produced only in CRC, but not normal stem cells, and metabolic stress is high in metastases, these data provide one of the mechanisms of how oncogenic Wnt signaling induces cancer cell adaptation and promotes metastatic cell outgrowth.

A related intriguing question is whether increased fitness of PROX1^{+} tumor cells reflects the role of PROX1 in normal tissues. The highest levels of Prox1 are found in lens fiber cells (Oliver et al., 1993). The lens is an avascular organ, located in a physiologically hypoxic and glucose-poor environment (Mathias et al., 1997; Trayhurn and Van Heyningen, 1972), and it is not fully understood how the lens maintains homeostasis in such conditions. Similarly, PROX1^{+} lymphatic vessels, unlike blood vessels, do not need basement membrane or pericytes to survive, grow in relatively hypoxic environment, and do not regress after removal of proliferative stimuli (Baluk et al., 2005). Thus, it seems plausible that PROX1 enhances adaptation of normal cells to unfavorable metabolic conditions.

An important observation of this study is the differential role of PROX1 in metastases versus primary tumors in advanced colorectal cancer. In our models, all of which carry mutations in oncogenic and tumor suppressor genes *APC*, *KRAS*, and *TP53*, PROX1 suppression decreased metastasis size and proliferation, whereas having little effect on the size or proliferation of primary tumors. Whereas the mechanisms are yet unknown, we propose that PROX1 is needed to provide a survival advantage to metabolically stressed cells. This is supported by the fact that CQ treatment is more effective in reducing growth of

Figure 6. Therapeutic Potential of Targeting PROX1

(A) PROX1 depletion in established metastases prevents further growth. SW480R/PROX1si cells, implanted intracecally into NOD-SCID; IL-2R$\gamma^{-/-}$ mice, were detected by in vivo bioluminescence imaging. Insert: macroscopic liver metastases in control SW480R/PROX1si mouse. The scale bar represents 750 μm. Two-way ANOVA; ***$p < 0.001$. Data are presented as mean ± SEM.

(B) PROX1 suppression does not affect weight of primary tumors. Data are presented as box and whiskers; Tukey appearance.

(C) PROX1 suppression prevents further growth of metastases. ***$p < 0.001$. Data are presented as box and whiskers; Tukey appearance.

(D) Inhibition of autophagy prevents PROX1-dependent adaptation to hypoxia. CQ, chloroquine. SW620 shCtr or shPROX1 cells were cultured for 72 hr in normoxic or hypoxic conditions in the presence or absence of 5 μM CQ. Staining for phosphohistone H3 (red), GLUT1 (green), and DNA (blue). The scale bar represents 50 μm.

(E) Quantification of cell proliferation. *$p < 0.05$; ***$p < 0.001$. Data are presented as mean ± SEM.

(F) Low-dose CQ does not affect metastases size. Quantification of metastases area in mice injected i.v. with tumor cells and treated with 10 mg/g CQ or PBS from day 7 post-implantation. Both necrotic and live tumor areas of metastases >100 μm^2 were quantified. Data are presented as box and whiskers; Tukey appearance.

(G) CQ treatment induces necrosis in metastases. Quantification of necrotic areas in liver metastases in mice treated with 10 mg/g CQ or PBS. Necrosis was evaluated at tumor-stromal interface, metastasis center, and in the entire lesion. **$p < 0.01$; ***$p < 0.001$. Data are presented as mean ± SEM.

(H) Low-dose CQ does not affect blood-vessel density. Left column: staining for endothelial marker endomucin (green), phosphohistone H3 (light blue), and DNA (blue). Yellow scattered line: highly vascularized metastatic area close to the liver stroma. White scattered line: the necrotic area. The scale bar represents 200 μm. Right column: staining for PROX1 (red), blood vessel marker endomucin (green), and DNA (blue). The scale bar represents 100 μm.

(I) CQ treatment reduces proliferation of PROX1^{+} metastases but has little effect on primary tumors. Staining for PH3 (light blue), PROX1 (red), and DNA (blue). White scattered lines, tumor area; white asterisk, areas of necrosis; yellow arrows, PH3^{+} cells. The scale bar represents 100 μm.

(J) Quantification of proliferation in orthotopic SW620 shCtr or shPROX1 primary tumors or metastases. Two-way ANOVA; ***$p < 0.001$. Data are presented as mean ± SEM.

(K) CQ treatment reduces proliferation of PROX1^{+} metastases. Staining for EdU (red), PROX1 (light blue), pimonidazole (green), and DNA (blue) of orthotopic SW620 shCtr or shPROX1 primary tumors or metastases following treatment with PBS or CQ. The scale bar represents 200 μm.

(L) Quantification of proliferation as determined by EdU incorporation. Data are presented as mean ± SEM.

(M) CQ treatment induces necrosis in PROX1^{+} metastases. Data are presented as mean ± SEM.

(N) Higher autophagic flux in metastases as compared to primary tumors. Staining for LC3B (red) and DNA (blue). Hypoxic areas are identified by staining for pimonidazole (green). The scale bar represents 25 μm.

(O) Quantification of LC3B^{+} cancer cells in primary tumors and metastases. Data are presented as mean ± SEM.

(P) Quantification of LC3B^{+} foci in individual cells. Two-way ANOVA; *$p < 0.05$; **$p < 0.01$. Data are presented as mean ± SEM.

(Q) Examples of images used for quantification in (O) and (P). Staining for LC3B (red) and DNA (blue). The scale bar represents 2 μm.

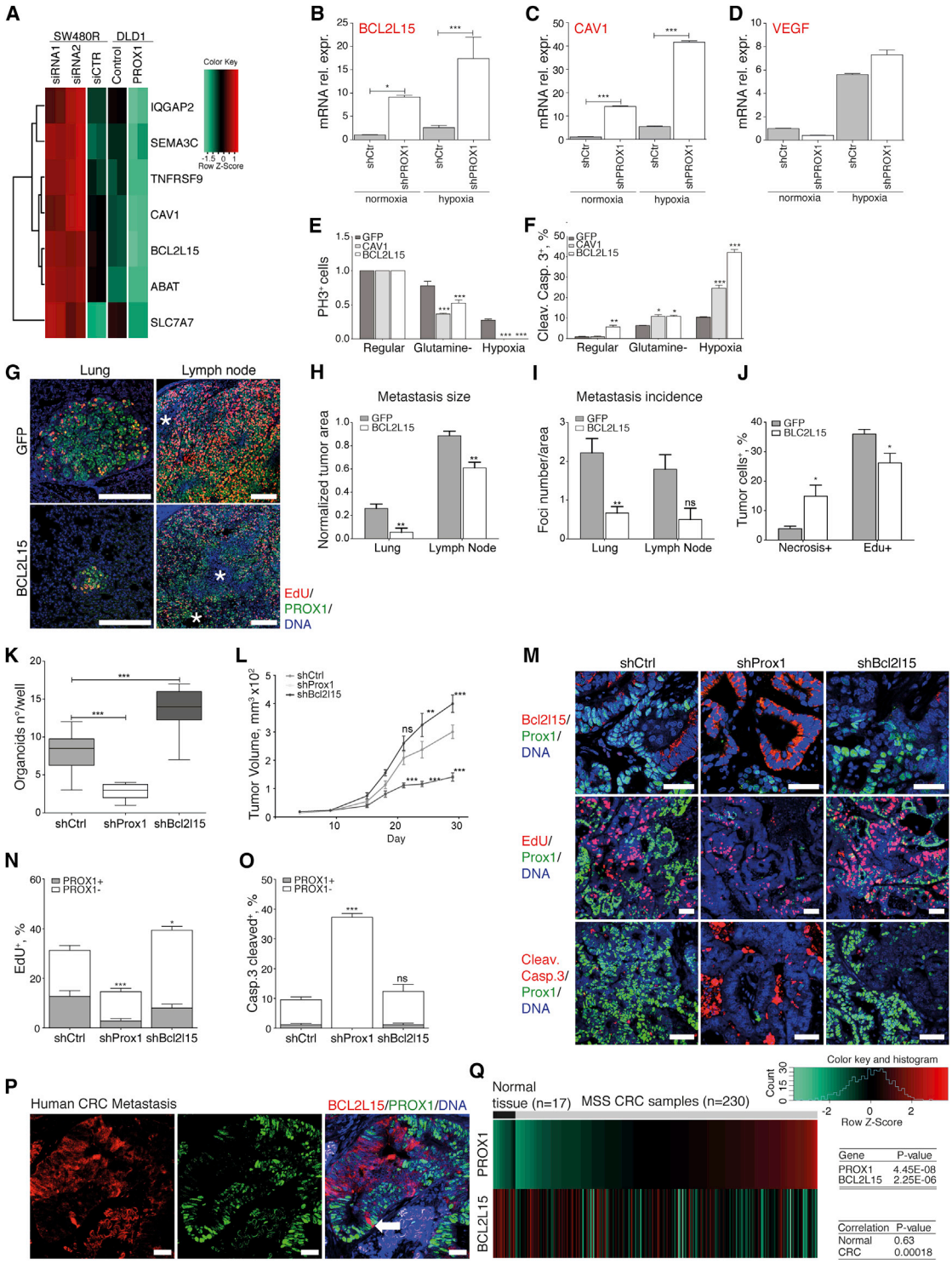

Figure 7. BCL2L15 Is a Direct PROX1 Effector Gene

(A) Heatmaps of selected PROX1 targets in two cells lines.

(B–D) BCL2L15 and CAV1 are induced in hypoxia in the absence of PROX1. Quantitative PCR analysis of the indicated transcripts. Cells were cultured in normoxia or hypoxia for 24 hr. Data are presented as mean ± SEM.

(E and F) BCL2L15 and CAV1 suppress cell proliferation and induce apoptosis in hypoxia. Cells were cultured for 72 hr in normoxia or 0.1% O_2. Proliferating or apoptotic cells were identified by staining for phosphohistone H3 or activated caspase-3. Two-way ANOVA; *$p < 0.05$; **$p < 0.01$; ***$p < 0.001$. Data are presented as mean ± SEM.

(legend continued on next page)

PROX1$^+$ metastasis versus primary tumors and that metastases have higher levels of autophagy. Interestingly, whereas generally PROX1 increases metastases size, PROX1$^+$ and PROX1$^-$ metastases have a comparable size in skeletal muscle (Figure 3E). These data indicate that metabolically active tissue such as skeletal muscle can complement the deficiency in PROX1. They also highlight important differences in metabolism of metastases versus primary tumors and further underscore a need to better understand and exploit such differences.

Previous studies documented a critical role of stromal inflammation, extracellular matrix, and chemokine/growth factor signaling for the successful outgrowth of cancer cells (Chaffer and Weinberg, 2011; Bhowmick, 2012; Zeelenberg et al., 2003). Our work reveals a cancer-type-specific mechanism of metastasis progression by demonstrating that the CRC-specific Wnt target gene PROX1 increases metabolic fitness of metastatic cancer stem cells. Importantly, all human and mouse models used in the study carry an activating mutation in *KRAS*, which underlies intrinsic or acquired resistance to targeted anti-EGFR therapies (Van Emburgh et al., 2014). PROX1 deficiency can therefore override advantages gained through the activation of KRAS signaling in Wnt^{high} cancer cells. Thus, targeting of PROX1 and PROX1-dependent pathways should be further explored for development of potential treatment approaches of PROX1$^+$ *KRAS* mutant, anti-EGFR-resistant CRC metastases.

EXPERIMENTAL PROCEDURES

Human Tumor Analyses

Use of human CRC samples was approved by the Canton of Vaud's ethics committee. See Supplemental Experimental Procedures for staining and tumor sample information.

Bioinformatics Analyses

The correlation analysis of PROX1 expression with cell differentiation, proliferation, and stem cell markers was based on GSE41258 data set (Sheffer et al., 2009). We used GSE33112 data set (de Sousa E Melo et al., 2011) to analyze PROX1 levels in Wnt^{high} and Wnt^{low} CSCs. See Supplemental Experimental Procedures for the detailed description. PROX1 and BCL2L15 expression was analyzed in 230 microsatellite stable colon tumors and 17 normal colon tissues from The Cancer Genome Atlas (TCGA) data set COAD UNC_IlluminaGA_RNASeqV2 (TCGA project: http://cancergenome.nih.gov/).

Cell Lines and Culture Conditions

SW620, SW480, and DLD1 (CCL-227, CCL-228, and CCL-221; ATCC) cells were used for generation of cell lines and spheroids as described in Supplemental Experimental Procedures. ECAR and OCR were measured in cells cultured for 24 hr prior to analysis according to the manufacturer's protocols (SeahorseBio), and all data were normalized to the total protein content.

Animal Studies

Experiments were approved by the Animal Ethics Committee of the Canton of Vaud or by the UK Home Office regulations. The complete list of mouse lines, genotyping, and other procedures are provided in Supplemental Experimental Procedures.

Staining Procedures

Staining procedures and list of antibodies are provided in Supplemental Experimental Procedures. Metastases were quantified using staining for human vimentin or KRT20. We detected cell proliferation for phosphohistone H3 (Cell Signaling Technology) and apoptosis by staining for cleaved caspase-3 (CST) or by TUNEL assay (R&D Systems). We used Axiovision Imager.Z1 or Zeiss LSM 510 META scanning confocal microscope for image acquisition and Bitplane IMARIS Suite 6.3.1 and Adobe Photoshop CS6 for image analyses.

RNA Isolation, Quantitative PCR, Microarray Analyses, and Western Blotting

We used RNeasy columns (QIAGEN) for RNA isolation and Agilent 2100 Bioanalyzer (Agilent) for RNA quality control. For transcriptome analyses, we used RNA from DLD1, DLD1-PROX1, or SW480R cells, transfected with 10 nM PROX1 siRNAs and AllStars control siRNAs (QIAGEN). Affymetrix Human Gene 1.0 ST arrays (Affymetrix) were used for gene-expression profiling.

See Supplemental Experimental Procedures for list of siRNAs and primers. We performed RT-PCR analyses on StepOnePlus or 7500-Fast real-time PCR Systems (Applied Biosystems) with SYBR Green PCR Master Mix (Applied Biosystems).

For western blotting, proteins were resolved by SDS-PAGE, transferred onto Immobilon-P, and detected with horseradish-peroxidase-conjugated secondary antibodies (Dako) and enhanced chemiluminescence (Thermo Fisher Scientific).

PROX1 ChIP-Seq and Reporter Analyses

Pools of three independent ChIP experiments and input DNA were used for sequencing (see Supplemental Experimental Procedures).

ChIP-seq data, generation of BCL2L15 luciferase reporter constructs, and their analyses are described in Supplemental Experimental Procedures.

(G) BCL2L15 limits growth of metastases. GFP- or BCL2L15-expressing SW620 cells were injected i.v., and metastases were analyzed 30 days later. Staining for PROX1 (green), EdU (red), and DNA (blue). The scale bar represents 100 μm.
(H) Quantification of metastasis size for data shown in (F). Data are presented as mean ± SEM.
(I) Metastasis incidence. Data are presented as mean ± SEM.
(J) BCL2L15 promotes tumor necrosis and reduces proliferation in metastatic PROX1$^+$ cells. Two-way ANOVA; *$p < 0.05$; **$p < 0.01$. Data are presented as mean ± SEM.
(K) Depletion of Bcl2l15 increases clonogenicity of intestinal *Apc$^{fl/fl}$;Kras^{G12D};Tp53$^{fl/fl}$;villin-CreERT2* (AKP) organoids. Colonies were quantified at day 15, following seeding of 3,000 single cells per well, transduced with a nontargeting shRNA (shCtrl) or shProx1. One-way ANOVA; ***$p < 0.001$. Data are presented as box and whiskers; Tukey appearance.
(L) Bcl2l15 depletion promotes tumor growth. shBcl2l15, control nontargeting shRNA (shCtrl), or shProx1-transduced organoid were implanted subcutaneously into NOD-SCID$\gamma^{-/-}$ mice. Two-way ANOVA; **$p < 0.01$; ***$p < 0.001$. Data are presented as mean ± SEM.
(M) Target protein expression, proliferation, and apoptosis in organoid-derived tumors. Staining for Prox1 (green), Bcl2l15, EdU or cleaved caspase-3 (red), and DNA (blue). The scale bar represents 25 μm.
(N) Quantification of cell proliferation in organoid tumors. Data are presented as mean ± SEM.
(O) Quantification of apoptosis in organoid tumors. One-way ANOVA; *$p < 0.05$; ***$p < 0.001$. Data are presented as mean ± SEM.
(P) Mutually exclusive localization of PROX1 and BCL2L15 in human CRC metastases. Staining for PROX1 (green), BCL2L15 (red), and DNA (blue). The scale bar represents 25 μm.
(Q) BCL2L15 mRNA is reduced in colon tumors and anticorrelates with PROX1 mRNA levels. Heatmap of PROX1 and BCL2L15 mRNA levels in CRC tumors and normal colon samples.

Statistical Analyses

We used Prism 5.0 for laboratory data analysis. p value ≤ 0.05 was considered to be statistically significant. Full description of statistical analyses is provided in Supplemental Experimental Procedures.

ACCESSION NUMBERS

The ArrayExpress accession numbers for the DLD1 or SW480R ± PROX1 microarray data reported in this paper are E-MTAB-2020 and E-MTAB-2021. The Gene Expression Omnibus submission accession number for the PROX1 ChIP-seq analysis performed on SW480R cells reported in this paper is GSE60390. The Cis-Regulatory Element Annotation System output relative to those data is accessible at http://bcf.isb-sib.ch/data/ragusa_et_al/PROX1vsInput_hg18.bed and http://bcf.isb-sib.ch/data/ragusa_et_al/.

SUPPLEMENTAL INFORMATION

Supplemental Information includes Supplemental Experimental Procedures, seven figures, and four tables and can be found with this article online at http://dx.doi.org/10.1016/j.celrep.2014.08.041.

ACKNOWLEDGMENTS

We thank P. Andreux and K. Schoonjans for help with metabolic experiments; I. Stamenkovic for critical comments; M. De Palma for help with lentivirus preparation; J. Huelsken for intestinal organoid protocols; S. Robin for villin-CreERT2 mice; M. Jaquet, C. Beauverd, and R. Haider for technical assistance; F. Derouet for tail vein injections; and A. Sabine for help with graphism. We thank Lausanne Genomics Technologies Facility, the Cellular Imaging Facility, Mouse Pathology Facility, and Mouse Animal Facility of the University of Lausanne. The work was supported by Swiss National Science Foundation (PPP0033-114898 to T.V.P. and 31003A-141225 to G.M.), Swiss Bridge Foundation, NCCR Molecular Oncology, Association for the International Cancer Research UK, Oncosuisse (KLS-02570-02-2010), CRUK, ERC investigator award "COLONCAN" (to O.J.S.), EU FP7 grant no. 278568 "PRIMES," and Medic Foundation.

Received: November 15, 2013
Revised: July 8, 2014
Accepted: August 19, 2014
Published: September 18, 2014

REFERENCES

Baluk, P., Tammela, T., Ator, E., Lyubynska, N., Achen, M.G., Hicklin, D.J., Jeltsch, M., Petrova, T.V., Pytowski, B., Stacker, S.A., et al. (2005). Pathogenesis of persistent lymphatic vessel hyperplasia in chronic airway inflammation. J. Clin. Invest. *115*, 247–257.

Bhowmick, N.A. (2012). Metastatic ability: adapting to a tissue site unseen. Cancer Cell *22*, 563–564.

Budinska, E., Popovici, V., Tejpar, S., D'Ario, G., Lapique, N., Sikora, K.O., Di Narzo, A.F., Yan, P., Hodgson, J.G., Weinrich, S., et al. (2013). Gene expression patterns unveil a new level of molecular heterogeneity in colorectal cancer. J. Pathol. *231*, 63–76.

Céspedes, M.V., Espina, C., García-Cabezas, M.A., Trias, M., Boluda, A., Gómez del Pulgar, M.T., Sancho, F.J., Nistal, M., Lacal, J.C., and Mangues, R. (2007). Orthotopic microinjection of human colon cancer cells in nude mice induces tumor foci in all clinically relevant metastatic sites. Am. J. Pathol. *170*, 1077–1085.

Chaffer, C.L., and Weinberg, R.A. (2011). A perspective on cancer cell metastasis. Science *331*, 1559–1564.

Clevers, H. (2013). The intestinal crypt, a prototype stem cell compartment. Cell *154*, 274–284.

Cunningham, D., Atkin, W., Lenz, H.J., Lynch, H.T., Minsky, B., Nordlinger, B., and Starling, N. (2010). Colorectal cancer. Lancet *375*, 1030–1047.

De Roock, W., De Vriendt, V., Normanno, N., Ciardiello, F., and Tejpar, S. (2011). KRAS, BRAF, PIK3CA, and PTEN mutations: implications for targeted therapies in metastatic colorectal cancer. Lancet Oncol. *12*, 594–603.

de Sousa E Melo, F., Colak, S., Buikhuisen, J., Koster, J., Cameron, K., de Jong, J.H., Tuynman, J.B., Prasetyanti, P.R., Fessler, E., van den Bergh, S.P., et al. (2011). Methylation of cancer-stem-cell-associated Wnt target genes predicts poor prognosis in colorectal cancer patients. Cell Stem Cell *9*, 476–485.

Dempsey, C.E., Dive, C., Fletcher, D.J., Barnes, F.A., Lobo, A., Bingle, C.D., Whyte, M.K., and Renshaw, S.A. (2005). Expression of pro-apoptotic Bfk isoforms reduces during malignant transformation in the human gastrointestinal tract. FEBS Lett. *579*, 3646–3650.

Dolznig, H., Rupp, C., Puri, C., Haslinger, C., Schweifer, N., Wieser, E., Kerjaschki, D., and Garin-Chesa, P. (2011). Modeling colon adenocarcinomas in vitro a 3D co-culture system induces cancer-relevant pathways upon tumor cell and stromal fibroblast interaction. Am. J. Pathol. *179*, 487–501.

Fearon, E.R. (2011). Molecular genetics of colorectal cancer. Annu. Rev. Pathol. *6*, 479–507.

Friedrich, T., Richter, B., Gaiser, T., Weiss, C., Janssen, K.P., Einwächter, H., Schmid, R.M., Ebert, M.P., and Burgermeister, E. (2013). Deficiency of caveolin-1 in Apc(min/+) mice promotes colorectal tumorigenesis. Carcinogenesis *34*, 2109–2118.

Haq, R., Shoag, J., Andreu-Perez, P., Yokoyama, S., Edelman, H., Rowe, G.C., Frederick, D.T., Hurley, A.D., Nellore, A., Kung, A.L., et al. (2013). Oncogenic BRAF regulates oxidative metabolism via PGC1α and MITF. Cancer Cell *23*, 302–315.

Hirschhaeuser, F., Menne, H., Dittfeld, C., West, J., Mueller-Klieser, W., and Kunz-Schughart, L.A. (2010). Multicellular tumor spheroids: an underestimated tool is catching up again. J. Biotechnol. *148*, 3–15.

Janiszewska, M., Suvà, M.L., Riggi, N., Houtkooper, R.H., Auwerx, J., Clément-Schatlo, V., Radovanovic, I., Rheinbay, E., Provero, P., and Stamenkovic, I. (2012). Imp2 controls oxidative phosphorylation and is crucial for preserving glioblastoma cancer stem cells. Genes Dev. *26*, 1926–1944.

Jung, P., Sato, T., Merlos-Suárez, A., Barriga, F.M., Iglesias, M., Rossell, D., Auer, H., Gallardo, M., Blasco, M.A., Sancho, E., et al. (2011). Isolation and in vitro expansion of human colonic stem cells. Nat. Med. *17*, 1225–1227.

Kimura, T., Takabatake, Y., Takahashi, A., and Isaka, Y. (2013). Chloroquine in cancer therapy: a double-edged sword of autophagy. Cancer Res. *73*, 3–7.

Koehler, A.N. (2010). A complex task? Direct modulation of transcription factors with small molecules. Curr. Opin. Chem. Biol. *14*, 331–340.

Kreso, A., van Galen, P., Pedley, N.M., Lima-Fernandes, E., Frelin, C., Davis, T., Cao, L., Baiazitov, R., Du, W., Sydorenko, N., et al. (2014). Self-renewal as a therapeutic target in human colorectal cancer. Nat. Med. *20*, 29–36.

Lu, M.H., Huang, C.C., Pan, M.R., Chen, H.H., and Hung, W.C. (2012). Prospero homeobox 1 promotes epithelial-mesenchymal transition in colon cancer cells by inhibiting E-cadherin via miR-9. Clin. Cancer Res. *18*, 6416–6425.

Martorell, Ò., Merlos-Suárez, A., Campbell, K., Barriga, F.M., Christov, C.P., Miguel-Aliaga, I., Batlle, E., Casanova, J., and Casali, A. (2014). Conserved mechanisms of tumorigenesis in the Drosophila adult midgut. PLoS ONE *9*, e88413.

Mathias, R.T., Rae, J.L., and Baldo, G.J. (1997). Physiological properties of the normal lens. Physiol. Rev. *77*, 21–50.

Merlos-Suárez, A., Barriga, F.M., Jung, P., Iglesias, M., Céspedes, M.V., Rossell, D., Sevillano, M., Hernando-Momblona, X., da Silva-Diz, V., Muñoz, P., et al. (2011). The intestinal stem cell signature identifies colorectal cancer stem cells and predicts disease relapse. Cell Stem Cell *8*, 511–524.

Mizushima, N., Yoshimori, T., and Levine, B. (2010). Methods in mammalian autophagy research. Cell *140*, 313–326.

Oliver, G., Sosa-Pineda, B., Geisendorf, S., Spana, E.P., Doe, C.Q., and Gruss, P. (1993). Prox 1, a prospero-related homeobox gene expressed during mouse development. Mech. Dev. *44*, 3–16.

Petrova, T.V., Nykänen, A., Norrmén, C., Ivanov, K.I., Andersson, L.C., Haglund, C., Puolakkainen, P., Wempe, F., von Melchner, H., Gradwohl, G.,

et al. (2008). Transcription factor PROX1 induces colon cancer progression by promoting the transition from benign to highly dysplastic phenotype. Cancer Cell *13*, 407–419.

Roth, A.D., Tejpar, S., Delorenzi, M., Yan, P., Fiocca, R., Klingbiel, D., Dietrich, D., Biesmans, B., Bodoky, G., Barone, C., et al. (2010). Prognostic role of KRAS and BRAF in stage II and III resected colon cancer: results of the translational study on the PETACC-3, EORTC 40993, SAKK 60-00 trial. J. Clin. Oncol. *28*, 466–474.

Sadanandam, A., Lyssiotis, C.A., Homicsko, K., Collisson, E.A., Gibb, W.J., Wullschleger, S., Ostos, L.C., Lannon, W.A., Grotzinger, C., Del Rio, M., et al. (2013). A colorectal cancer classification system that associates cellular phenotype and responses to therapy. Nat. Med. *19*, 619–625.

Sasaki, K., Tsuno, N.H., Sunami, E., Kawai, K., Hongo, K., Hiyoshi, M., Kaneko, M., Murono, K., Tada, N., Nirei, T., et al. (2012). Resistance of colon cancer to 5-fluorouracil may be overcome by combination with chloroquine, an in vivo study. Anticancer Drugs *23*, 675–682.

Sato, T., Stange, D.E., Ferrante, M., Vries, R.G., Van Es, J.H., Van den Brink, S., Van Houdt, W.J., Pronk, A., Van Gorp, J., Siersema, P.D., and Clevers, H. (2011). Long-term expansion of epithelial organoids from human colon, adenoma, adenocarcinoma, and Barrett's epithelium. Gastroenterology *141*, 1762–1772.

Schepers, A.G., Snippert, H.J., Stange, D.E., van den Born, M., van Es, J.H., van de Wetering, M., and Clevers, H. (2012). Lineage tracing reveals Lgr5+ stem cell activity in mouse intestinal adenomas. Science *337*, 730–735.

Sheffer, M., Bacolod, M.D., Zuk, O., Giardina, S.F., Pincas, H., Barany, F., Paty, P.B., Gerald, W.L., Notterman, D.A., and Domany, E. (2009). Association of survival and disease progression with chromosomal instability: a genomic exploration of colorectal cancer. Proc. Natl. Acad. Sci. USA *106*, 7131–7136.

Skog, M., Bono, P., Lundin, M., Lundin, J., Louhimo, J., Linder, N., Petrova, T.V., Andersson, L.C., Joensuu, H., Alitalo, K., and Haglund, C.H. (2011). Expression and prognostic value of transcription factor PROX1 in colorectal cancer. Br. J. Cancer *105*, 1346–1351.

Sonoshita, M., Aoki, M., Fuwa, H., Aoki, K., Hosogi, H., Sakai, Y., Hashida, H., Takabayashi, A., Sasaki, M., Robine, S., et al. (2011). Suppression of colon cancer metastasis by Aes through inhibition of Notch signaling. Cancer Cell *19*, 125–137.

Spaderna, S., Schmalhofer, O., Wahlbuhl, M., Dimmler, A., Bauer, K., Sultan, A., Hlubek, F., Jung, A., Strand, D., Eger, A., et al. (2008). The transcriptional repressor ZEB1 promotes metastasis and loss of cell polarity in cancer. Cancer Res. *68*, 537–544.

Steffensen, K.R., Holter, E., Båvner, A., Nilsson, M., Pelto-Huikko, M., Tomarev, S., and Treuter, E. (2004). Functional conservation of interactions between a homeodomain cofactor and a mammalian FTZ-F1 homologue. EMBO Rep. *5*, 613–619.

Todaro, M., Gaggianesi, M., Catalano, V., Benfante, A., Iovino, F., Biffoni, M., Apuzzo, T., Sperduti, I., Volpe, S., Cocorullo, G., et al. (2014). CD44v6 is a marker of constitutive and reprogrammed cancer stem cells driving colon cancer metastasis. Cell Stem Cell *14*, 342–356.

Trayhurn, P., and Van Heyningen, R. (1972). The role of respiration in the energy metabolism of the bovine lens. Biochem. J. *129*, 507–509.

Truninger, K., Menigatti, M., Luz, J., Russell, A., Haider, R., Gebbers, J.O., Bannwart, F., Yurtsever, H., Neuweiler, J., Riehle, H.M., et al. (2005). Immunohistochemical analysis reveals high frequency of PMS2 defects in colorectal cancer. Gastroenterology *128*, 1160–1171.

Van Emburgh, B.O., Sartore-Bianchi, A., Di Nicolantonio, F., Siena, S., and Bardelli, A. (2014). Acquired resistance to EGFR-targeted therapies in colorectal cancer. Mol. Oncol. Published online May 14, 2014. http://dx.doi.org/10.1016/j.molonc.2014.05.003.

White, E. (2012). Deconvoluting the context-dependent role for autophagy in cancer. Nat. Rev. Cancer *12*, 401–410.

Wiener, Z., Högström, J., Hyvönen, V., Band, A.M., Kallio, P., Holopainen, T., Dufva, O., Haglund, C., Kruuna, O., Oliver, G., et al. (2014). Prox1 Promotes Expansion of the Colorectal Cancer Stem Cell Population to Fuel Tumor Growth and Ischemia Resistance. Cell Rep. Published online September 18, 2014. http://dx.doi.org/10.1016/j.celrep.2014.08.034.

Wolf, M.J., Hoos, A., Bauer, J., Boettcher, S., Knust, M., Weber, A., Simonavicius, N., Schneider, C., Lang, M., Stürzl, M., et al. (2012). Endothelial CCR2 signaling induced by colon carcinoma cells enables extravasation via the JAK2-Stat5 and p38MAPK pathway. Cancer Cell *22*, 91–105.

Zeelenberg, I.S., Ruuls-Van Stalle, L., and Roos, E. (2003). The chemokine receptor CXCR4 is required for outgrowth of colon carcinoma micrometastases. Cancer Res. *63*, 3833–3839.

PROX1 promotes metabolic adaptation and fuels outgrowth of Wnt^{high} metastatic colon cancer cells

Ragusa et al.,

Supplemental Information

Supplemental Figures

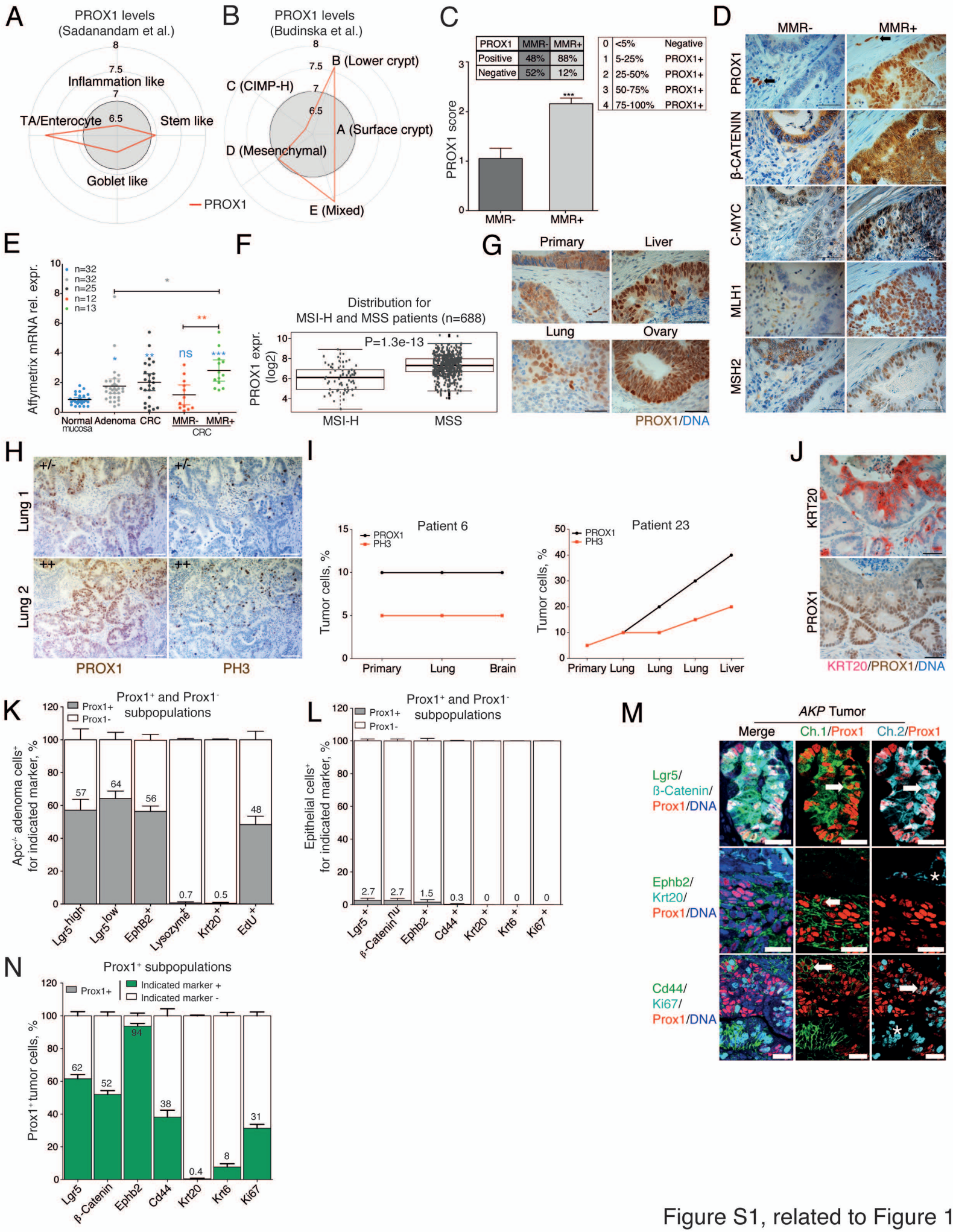

Figure S1, related to Figure 1

Figure S1, related to Figure 1. Analyses of PROX1 expression in human and mouse CRC. (A, B) PROX1 is preferentially expressed in Wnt^{high} types of CRC tumors. Molecular classification according to (Sadanandam et al., 2013) and (Budinska et al., 2013). PROX1 expression (red line) is expressed as log_2. CIMP-H, CpG island methylator phenotype-high. (C) PROX1 protein is higher in MMR^+ CRC tumors. Histological score for PROX1 in MMR^+ (*n*=125) and MMR^- (*n*=35) CRC samples. Scoring is based on the percentage of strongly nuclear PROX1-positive cells, normalized to the total number of cancer cells. Student *t*-test: ***, *P*<0.001. Mean ± SEM. (D) Examples of PROX1 expression in MMR^+ and MMR^- tumors. Staining for PROX1, ß-catenin (CTNNB1), CMYC, MLH1 and MSH2 (brown), and DNA (blue). Scale bar, 50µm. (E) *PROX1* mRNA levels in normal colonic mucosa, adenoma samples, all CRCs, and those stratified according to their MMR status. Dataset by (Sabates-Bellver et al., 2007) was used for the analysis. One-way ANOVA, *, *P*<0.05; **, *P*<0.01. Mean ± SEM. (F) Correlation of PROX1 mRNA with MSI/MSS status in PETACC-3 database for 688 CRC primary tumors (Roth et al., 2010). *P*=1.3e-13. Log. expression values, 1.5xIQR. (G) Example of $PROX1^-$ primary CRC with corresponding $PROX1^+$ metastases. Staining for PROX1 (brown) and DNA (blue). Scale bar, 100µm. (H) Expression levels of PROX1 correlate with proliferation of human metastases. Chromogenic staining of serial sections of lung metastases for PROX1 and phosphohistone H3 (brown) and DNA (blue). Scale bar, 200µm. Upper row, low PROX1 expression and proliferation; lower row, high PROX1 expression and proliferation. (I) Examples of PROX1 and phosphohistone H3 scores in two patients. (J) PROX1 levels in human CRC metastases are anti-correlated with differentiation marker KRT20. Staining for KRT20 (red), PROX1 (brown) and DNA (blue). Scale bar, 50µm. (K) Quantification of $Prox1^+$ cells in the indicated

subsets of cells in *Apc$^{f/f}$;Lgr5-EGFP-Ires-CreERT2* adenomas. Mean ± SEM. (L) Quantification of Prox1^{+} cells in the indicated subsets of normal small intestinal cells in *AKP* mice. Mean ± SEM. (M) Expression pattern of Prox1, stem/progenitor and proliferation markers in *AKP* intestinal tumors. Prox1 (red), Lgr5, EphB2 and Cd44 (green), β-Catenin, Krt20 and Ki67 (light blue) and DNA (blue). White arrows indicate Prox1^{+}/marker^{+} cells. White asterisk indicate Prox1^{-}/marker^{+} cells. Scale bar, 20μm. (N) Quantification of Prox1^{+} cells in the indicated subsets of cells of *AKP* tumors. Mean ± SEM.

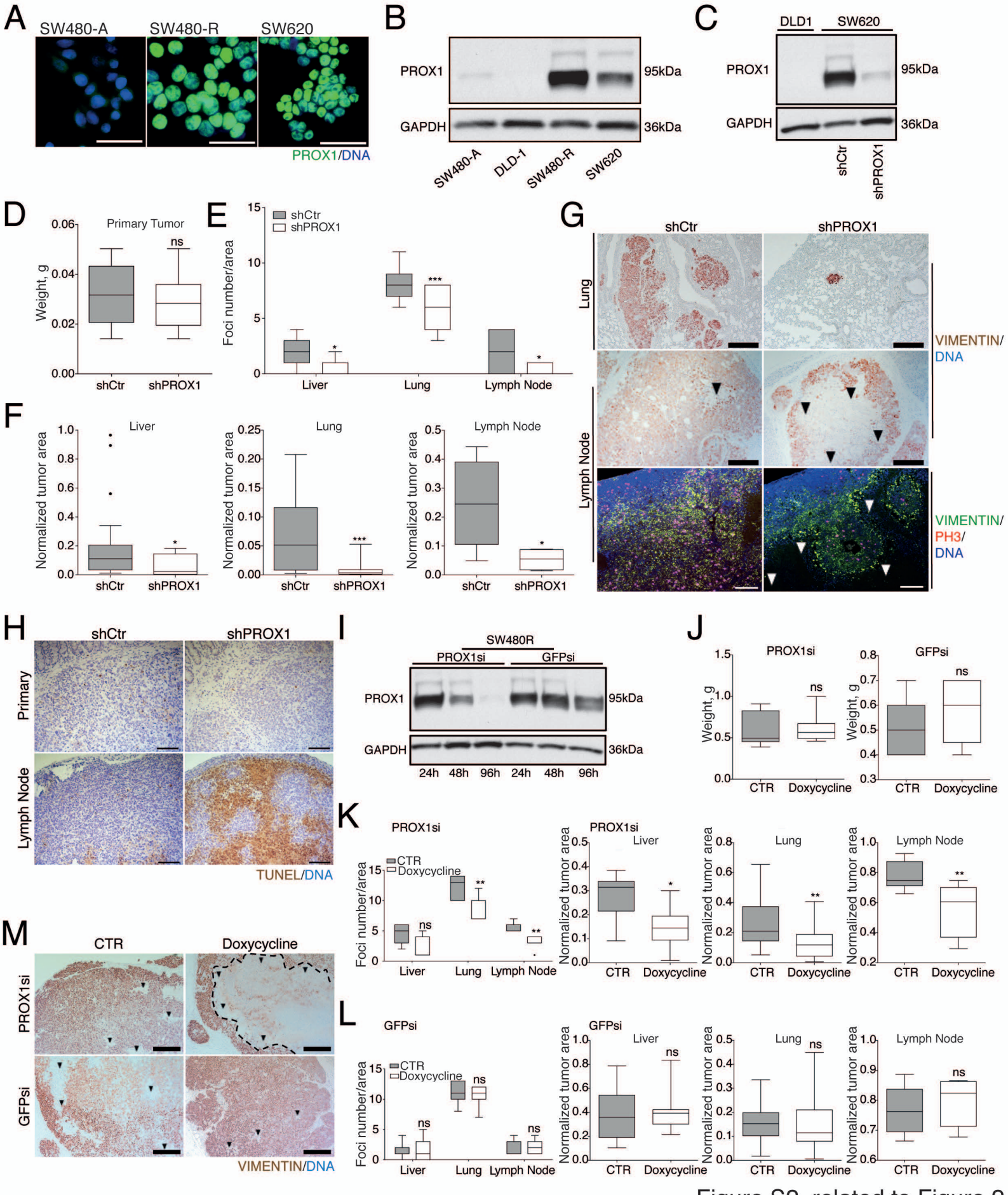

Figure S2, related to Figure 2

Figure S2, related to Figure 2. PROX1 promotes colon cancer metastasis. (A) SW620 cells, derived from lymph node metastases of colon adenocarcinoma express high levels of PROX1.Staining for PROX1 (green) and DNA (blue). Scale bar, 20μm. (B) Western blotting for indicated proteins. Parental SW480-A cell line and DLD1 cells express low levels of PROX1; parental SW480-R cells express high levels. (C) Efficient *in vitro* down-regulation of PROX1 in SW620 shPROX1 cells. Western blot for the indicated proteins. (D) PROX1 depletion does not affect growth of primary tumors. Student t-test, ns. Tukey appereance. (E) Increased incidence of SW620 shCtr metastases. Metastatic foci are identified by staining for human vimentin. One-way ANOVA: *, $P<0.05$; ***, $P<0.005$. Tukey appereance. (F) Depletion of PROX1 decreases size of metastases. Individual metastasis size was determined by dividing total vimentin$^+$ areas by the number of lesions and normalized to the total surface analyzed. Student t-test: *, $P<0.05$; ***, $P<0.005$. Tukey appereance. (G, H) shPROX1 metastases have decreased proliferation and increased cell death. (G) Histology of lung and lymph node SW620 metastases. Staining for human vimentin (brown) and DNA (blue); or vimentin (green), phosphohistone H3 (red) and DNA (blue). Arrowheads: necrotic areas. Scale bar 200μm. (H) Comparable apoptosis in PROX1$^-$ and PROX1$^+$ primary tumors and increased apoptosis in PROX1$^-$ metastases. TUNEL staining (brown) and DNA (blue). Scale bar, 200μm. (I) Treatment with doxycycline reduces PROX1 levels in SW480R-PROX1si cells, but not in the control SW480R-GFPsi cells. Western blotting for the indicated proteins. (J) Inducible depletion of PROX1 does not affect growth of primary tumors. Dissected tumor weight. Student *t*-test, ns. Tukey appereance. (K) Doxycycline treatment decreases the incidence of SW480R/ PROX1si metastases, and reduces individual metastases size. Individual metastasis size was determined by dividing the total metastasic areas by

the number of metastases and normalizing to tissue area analyzed. Student t-test, *, $P<0.05$; **, $P<0.01$. One-way ANOVA, **, $P<0.01$. Tukey appereance. (L) Doxycycline treatment does not affect metastasis in SW480R/GFPsi cells. Cancer cells were identified with human vimentin^{+} staining. Student *t*-test and One-way ANOVA, ns. Tukey appereance. (M) Microscopic appearance of SW480R metastatic lymph nodes in the indicated tumor types. Staining for vimentin (brown), and counterstained for DNA (blue). Black arrowheads mark necrotic areas. Scale bar, 200 μm.

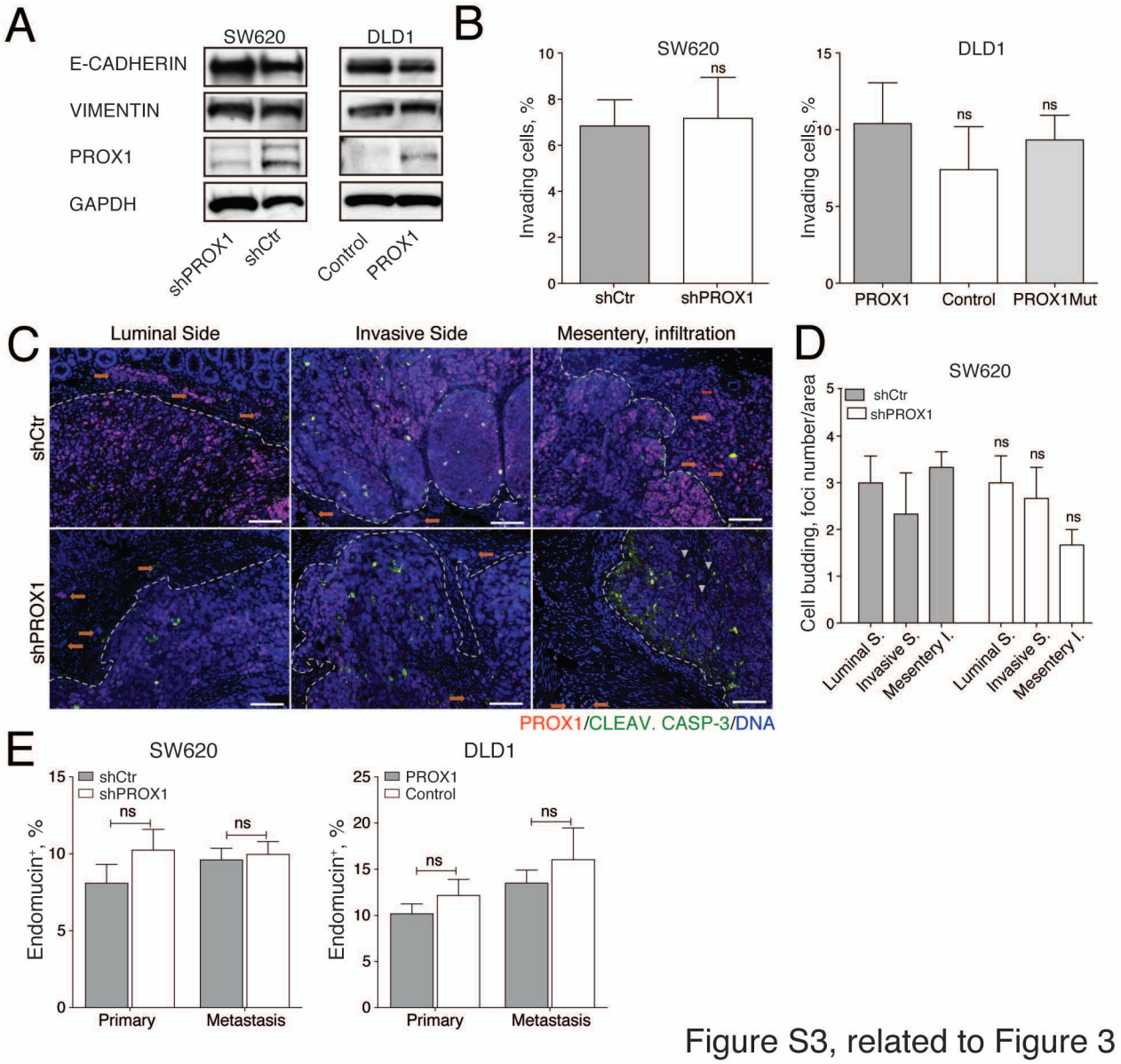

Figure S3, related to Figure 3

Figure S3, related to Figure 3. PROX1 does not induce EMT, local invasion or angiogenesis. (A) PROX1 does not modulate EMT *in vitro*. Western blotting for epithelial marker E-cadherin, mesenchymal marker vimentin, PROX1 and GAPDH, in cultured SW620 shCtr or shPROX1 cells and DLD1-PROX1 or DLD1 control cells. (B) PROX1 does not affect CRC invasion *in vitro*. Matrigel invasion assay of SW620 shCtr or shPROX1 (left) and DLD1-PROX1 or DLD-1-control (right) cells. Invasion is indicated as percentage of transmigrated cells, normalized to the total number of plated cells. Student *t*-test (SW620) and one-way ANOVA (DLD1), ns. Mean ± SEM. (C) Absence of gross alterations in the pattern of primary tumor invasion in SW620 shCtr and shPROX1 tumors. Staining for PROX1 (pink), active caspase-3 (green) and DNA (blue). Orange arrows, invasive strands of cells. White arrowheads, necrotic areas. Scale bar, 100μm. (D) Semi-quantitative analysis of invasion in tumors. Invasion into indicated tumor sides is expressed as cell budding and invasive strands foci number over total tumor areas analyzed. One-way ANOVA, ns. Mean ± SEM. (E) Comparable blood vascular density in primary or metastatic $PROX1^{+}$ or $PROX1^{-}$ tumors. Endothelial cells were identified by staining for endomucin. Vascular index is expressed as total vessel surface per tumor area. One-way ANOVA, ns. Mean ± SEM.

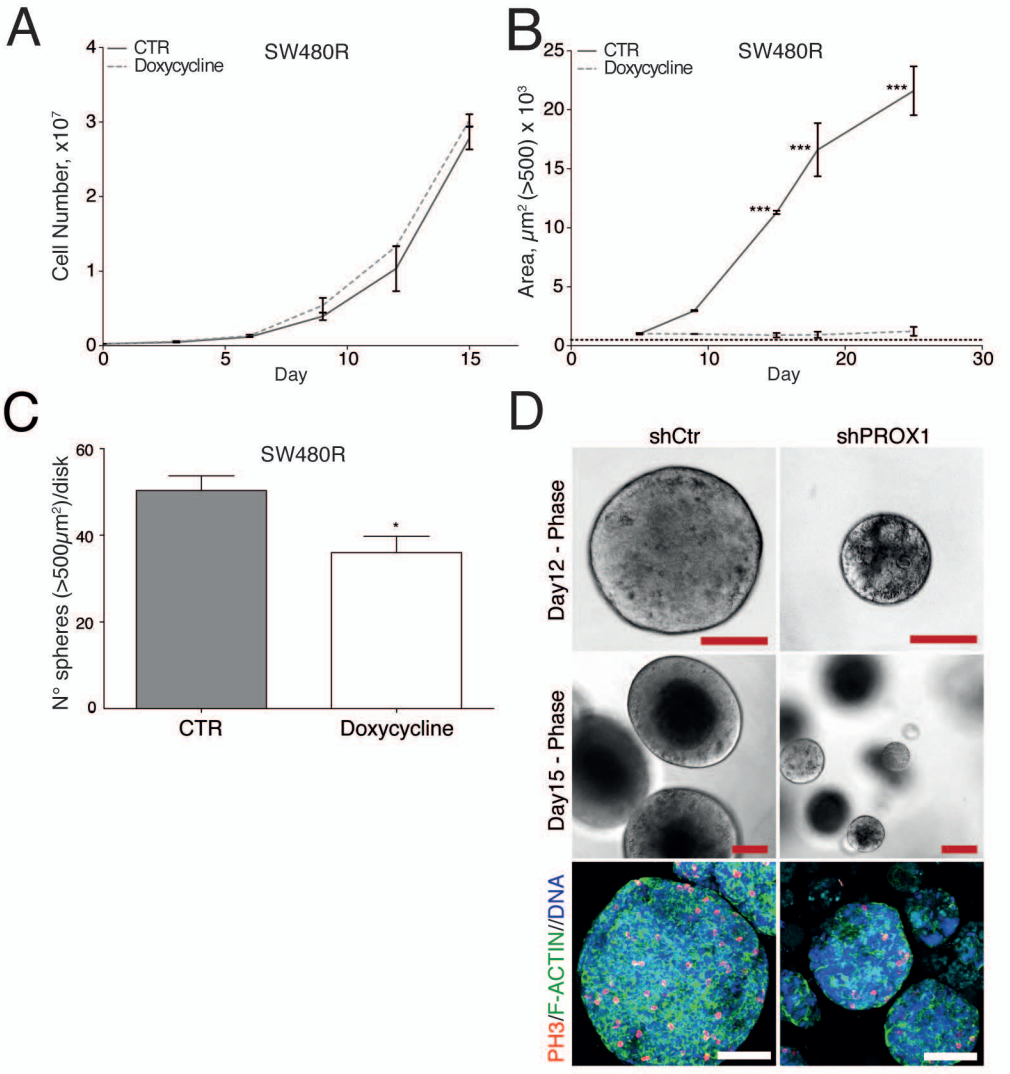

Figure S4, related to Figure 4

Figure S4, related to Figure 4. Effects of PROX1 depletion on growth of CRC cells in 3D. (A) Doxycycline treatment does not affect growth of SW480R/PROX1si cells under 2D conditions. *In vitro* growth curves of SW480R/PROX1si cells treated with PBS (control, CTR) or doxycycline. Mean ± SEM. (B) PROX1 suppression decreases growth of SW480R spheroids. Size of SW480R/PROX1si individual spheroids treated with doxycycline or PBS. Two-way ANOVA, ***, $P<0.001$. Mean ± SEM. (C) Doxycycline treatment decreases the incidence of SW480R/PROX1si spheroids. Total number of spheroids >500μm^2. Student *t*-test, *, $P<0.05$. Mean ± SEM. (D) Suppression of PROX1 reduces growth of tumor spheroids. Microscopic phase contrast appearance of SW620-shCtr or shPROX1 spheroids at day 12 (upper row) and 15 (middle row). Scale bar, 100μm. Lower row: increased proliferation of SW620 shCtr spheroids. Whole mount staining for phosphohistone H3 (red), F-actin (green), and DNA (blue). Scale bar, 100μm.

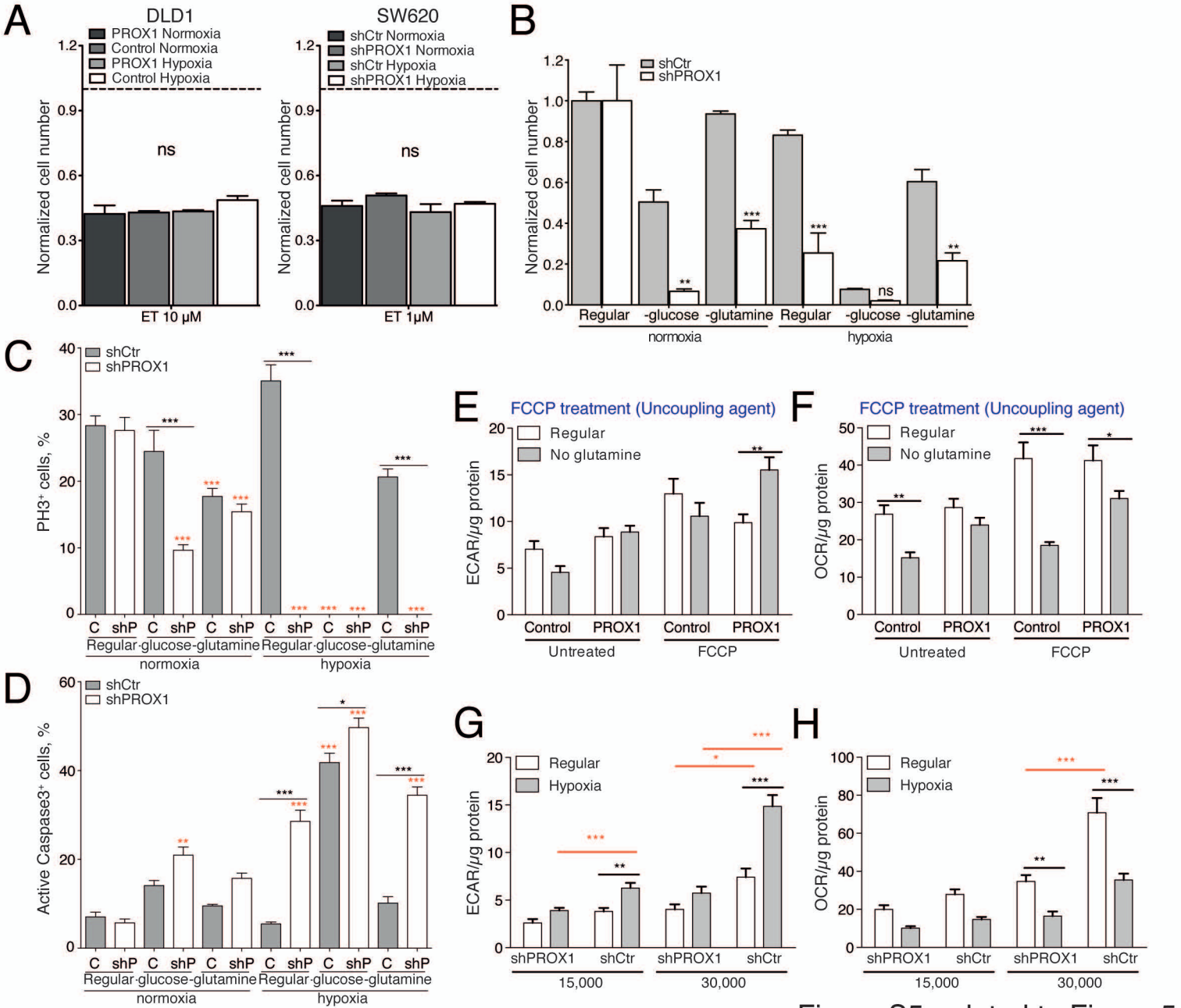

Figure S5, related to Figure 5

Figure S5, related to Figure 5. PROX1 promotes resistance and metabolic adaptation to hypoxia and nutrient deprivation. (A) Etoposide induces cell death both $PROX1^{+}$ and $PROX1^{-}$ cells. DLD1 PROX1 or Control, and SW620 shPROX1 or shCtr cells were cultured for 72 hours in the presence of 10 or 1μM etoposide (ET) and cell number was determined using Cell Titer Blue (CTB) assay. Data of each culture condition are normalized to CTB values in untreated cells. One-way ANOVA, ns. Mean ± SEM. (B) Depletion of PROX1 in SW620 cells decreases cell number in hypoxia and low-nutrient conditions. Cell number was determined by CyQuant assay. Two-way ANOVA; **, $P<0.01$; ***, $P<0.001$. Mean ± SEM. (C) SW620 shCtr but not shPROX1 cells continue to proliferate in hypoxia or low nutrient conditions. Proliferating cells were determined by staining for phosphohistone H3. Mean ± SEM. (D) SW620 shCtr cell evade apoptosis in hypoxia or low nutrient conditions. Percentage of apoptotic cells, as determined by staining for cleaved caspase-3. One-way ANOVA, comparing same conditions in shCtr versus shPROX1 cells, black *, $P<0.05$; ***, $P<0.001$; Two-way ANOVA, treatment versus normal culture conditions of same cell type, red **, $P<0.01$, ***, $P<0.001$. Mean ± SEM. (E) DLD1 PROX1 cells cultured in low glutamine have similar glycolysis rates in comparison to control cells. Inhibition of mitochondrial respiration with uncoupling agent FCCP induces higher glycolysis in PROX1 cells only. (F) Higher oxidative phosphorylation in glutamine-starved DLD1 PROX1 cells. (G) Higher glycolysis rates in SW620 shCtr cells cultured in hypoxia as compared to SW620 shPROX1 cells. (H) Decreased oxygen consumption rates in SW620 shCtr and shPROX1 cultured under hypoxic conditions. Two-way ANOVA, * $P<0.05$, ** $P<0.005$, *** $P<0.001$; red * PROX1+ versus PROX1- cells in indicated condition, black *, significant change of the same cell type in switched condition. Mean ± SEM.

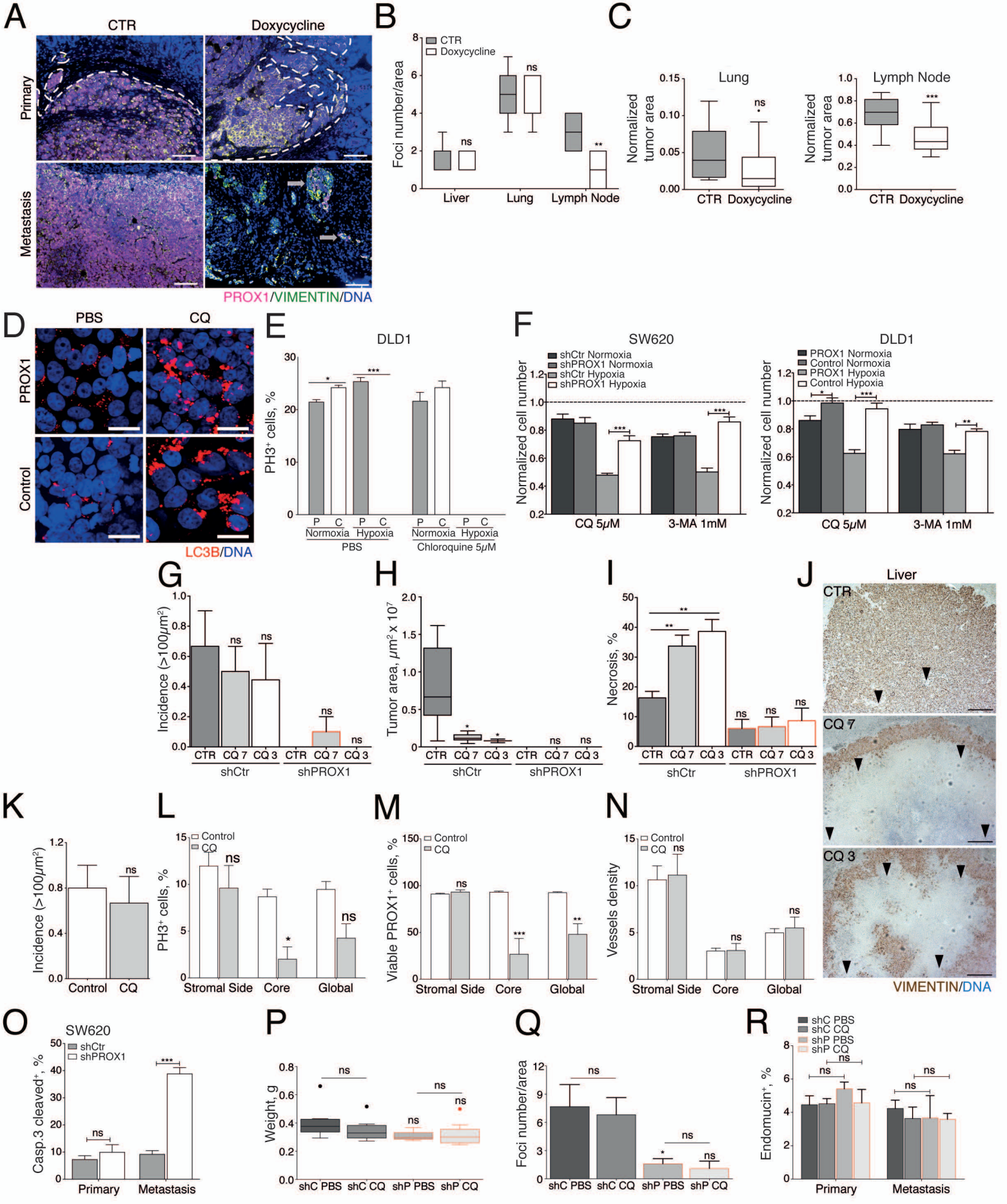

Figure S6, related to Figure 6

Figure S6, related to Figure 6. Therapeutic potential of targeting PROX1. (A) PROX1 protein is reduced both in primary tumors and metastases upon administration of doxycycline. SW480R/PROX1si cells were implanted into caecum of NOD-scid; IL-2Rγ-/- mice and doxycycline was administered 30 day after the implantation, when metastases were already detectable. Staining for PROX1 (red), vimentin (green) and DNA (blue). White dashed line, tumor margins. White arrows, $PROX1^{+}$ infiltrated cells escaping inhibition. Scale bar, 100μm. (B) Effects of PROX1 depletion in established metastases. Two-way ANOVA, **, $P<0.01$. $n=11$ per group. Tukey appereance. (C) PROX1 depletion reduces size of individual lung and lymph node metastases. Tumor cells were identified by staining for human vimentin. Individual metastasis size was determined by dividing the total metastasic areas by the number of metastases and normalizing to tissue area analyzed. Student t-test, ***, $P<0.01$. Tukey appereance. (D) Chloroquine (CQ) induces enlarged autophagosome in hypoxic colon cancer cells. Staining of DLD1 PROX1 and Control cells for the autophagosome component LC3B (red) and DNA (blue). Scale bar 25μm. (E) Chloroquine (CQ) suppresses PROX1-dependent cell adaptation to hypoxia. Quantification of cell proliferation as determined by staining for phosphohistone H3 in DLD1 PROX1 (P) and Control (C) cells. Mean ± SEM. (F) Autophagy inhibitors suppress $PROX1^{+}$ cell growth in hypoxia. DLD1 or SW620 cells were cultured in the absence and in the presence of chloroquine (CQ) or 3-methyl adenine (3-MA) for 72 hours in normoxia or hypoxic conditions and cell number was determined using Cell Titer Blue assay (CTB). Data of each culture condition are normalized to CTB values in untreated cells. PROX1- cells appear unaffected because of low proliferation and high apoptosis in hypoxic conditions already without treatment. Mean ± SEM. (G) 40 mg/kg chloroquine treatment does not affect incidence of liver metastases. Mean ±

SEM. (H) 40 mg/kg chloroquine treatment reduces the size and (I) increases necrosis in liver metastases. Metastases >100μm^2 were used for quantification. Tumor cells were identified by staining for human vimentin. One-way ANOVA, *, P<0.05, ** P<0.01, *** P<0.001. Tukey appereance (H). Mean ± SEM (I). (J) Chloroquine induces central necrosis in SW620 shCtr liver metastases. Cells were injected into the tail vein, and CQ or PBS was administered at day 3 (CQ 3) or 7 (CQ 7) post-injection. Tumor cells were identified by staining for human vimentin. Black arrowheads indicate necrotic areas. Scale bar, 200μm. (K) 10 mg/kg chloroquine treatment does not affect the incidence of liver metastases. Metastases >100μm^2 were quantified. Tumor cells were identified by staining for human vimentin. Student t-test, ns. Mean ± SEM. (L) Quantification of phosphohistone H3$^+$ cells in liver metastases in mice treated with 10 mg/kg CQ or PBS at tumor-stromal interface, metastasis center and globally. Mean ± SEM. (M) Quantification of PROX1$^+$ cells in liver metastases, and (N) quantification of vascular density. Blood vessels were identified by staining for endomucin. Two-way ANOVA, *, P<0.05; **, P<0.01; ***, P<0.001. Mean ± SEM. (O) Comparable apoptosis rates in PROX1$^-$ and PROX1$^+$ primary tumors and high apoptosis in PROX1$^-$ metastases. Apoptosis was quantified in SW620 shCtr and shPROX1 tumors by staining for cleaved capase-3. Two-Way ANOVA, ***, P<0.001. Mean ± SEM. (P) Autophagy inhibition does not affect growth of primary tumors. SW620 PROX1$^+$ or PROX1$^-$ cells were injected intracecally and mice were treated with PBS or 10 mg/kg/day CQ starting at day 9th post injection. Tukey appereance. (Q) Chloroquine treatment does not affect number of metastatic foci in orthotopic model. One-Way ANOVA, * P<0.05. Mean ± SEM. (R) Chloroquine treatment does not affect tumor vascular density, as determined by staining for endomucin. Two-Way ANOVA, ns. Mean ± SEM.

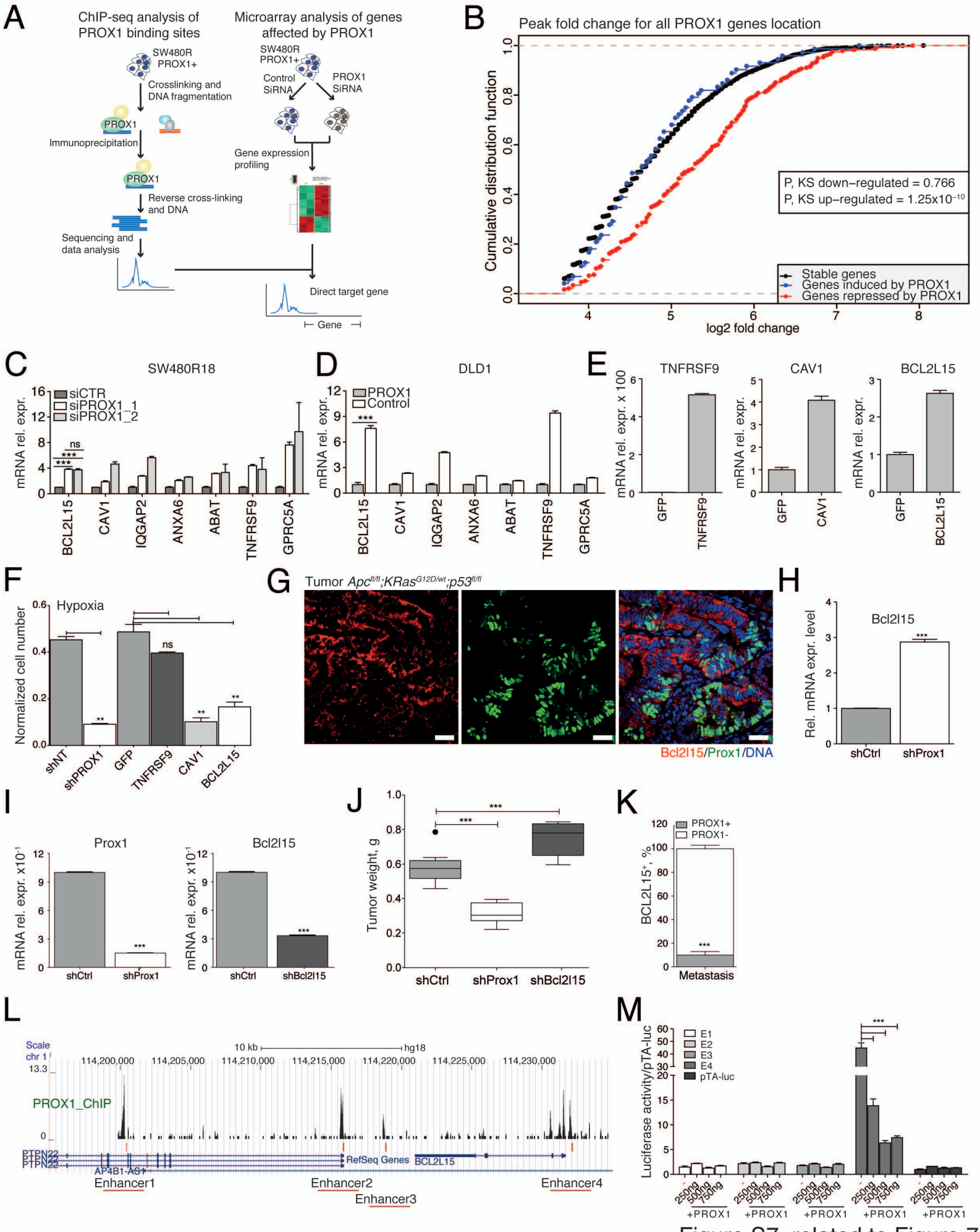

Figure S7, related to Figure 7

Figure S7, related to Figure 7. Molecular mechanisms of PROX1 in colorectal cancer. (A) Outline of experiments for the identification of PROX1 direct target genes. (B) PROX1 preferentially binds near PROX1-repressed genes. Cumulative distribution function of binding site intensity (as $\log_2$ fold enrichment over input) for PROX1, stratified by the set of genes up- or down-regulated by PROX1 or a reference set of stable genes in the corresponding knock-down experiment. *P*-values are relative to Kolmogorov-Smirnow tests of equal distribution as the reference. (C, D) Validation of microarray analysis. qPCR analysis for selected genes in SW480R transfected with two different PROX1 siRNAs and DLD1 $PROX1^+$ or $PROX1^-$ cells. Two-Way ANOVA, ***, $P<0.001$. Mean ± SEM. (E) Validation of TNFRSF9, BCL2L15 or CAV1 expression in SW620 TNFRSF9, BCL2L15, CAV1 or control GFP cell lines. qPCR analysis of the indicated transcripts. Mean ± SEM. (F) Overexpression of PROX1 targets BCL2L15 and CAV1, but not TNFRSF9, mimics the effects of PROX1 depletion in $PROX1^+$ SW620 cells cultured in hypoxia. SW620 transduced with shNT, not targeting, or shPROX1 lentiviruses were used as negative and positive controls. Cell number was determined by CyQuant DNA based assay after 72 hours. Two-way ANOVA, **, $P<0.01$. Mean ± SEM. (G) Inverse localization of Prox1 and Bcl215 protein in *AKP* intestinal tumor. Staining for Bcl2l15 (red), Prox1 (green), and DNA (blue). Scale bar, 50μm. (H) Prox1 depletion induces Bcl2l15 expression in *AKP* organoids *in vitro*. mRNA levels at day 5 post transduction. Student *t*-test, *** $P<0.001$. Mean ± SEM. (I) qPCR validation of Prox1 or Bcl2l15 suppression in *AKP* shCtrl, shProx1 and shBcl2l15 after puromycin selection. mRNA levels. Student *t*-test, *** $P<0.001$. Mean ± SEM. (J) shBcl2l15 *AKP* organoids form larger tumors. shProx1 and shCtrl organoids were used as controls. One-Way ANOVA, *** $P<0.001$. Tukey appereance. (K) The majority of

BCL2L15^{+} cells in human colorectal cancer metastases does not express PROX1. Lung metastasis, n=5. Student t-test, ***, P<0.001. Mean ± SEM. (L) PROX1 binding sites in BCL2L15 locus, used for the luciferase reporter analyses. (M) PROX1 represses the activity of BCL2L15 enhancer 4. SW480A25 cells were transfected with the reporters or control pTAL vector plasmid and an expression vector for PROX1. Luciferase activity was measured 36 hours after the transfection, and is expressed as fold increase over the pTAL control values. Two-Way ANOVA, *** P<0.001. Mean ± SEM.

Potential target genes of PROX1 in DLD1 and SW480R cells

ABAT, BCL2L15, CAV1, IQGAP2, SEMA3C, SLC7A7 and TNFRSF9 are the genes with fold change greater than 2 folds, and have PROX1 binding in their vicinity

Genes repressed by PROX1 in two lines	Fold change in SW480R-siPROX1 1	Fold change in SW480R-siPROX1 2	Fold change in DLD1 cells	PROX1 binding in 50Kb upstream to 50Kb downstream
ABAT	2.332721376	2.223949456	1.650478677	+
ANXA1	2.314210343	2.29464345	1.905916613	+
ANXA6	1.838318189	2.27073681	1.631852884	+
AP1S2	2.657488595	2.460179361	1.757789726	+
BCL2L15	2.540603961	2.354974601	4.118251678	+
C3orf52	1.566523595	1.574714186	1.598285901	+
CAV1	2.041578442	2.91603897	2.323729278	+
CDRT1	1.973770158	1.965092876	2.432281991	+
CLIC5	1.571001437	1.78584083	2.280835659	+
CYBRD1	2.769060356	1.526339613	1.501348083	+
EMP1	3.680347519	3.413536078	1.70935909	+
EPAS1	6.280913932	4.188604014	1.965151447	-
GBP1	2.084760999	1.846328166	1.832850355	+
GBP3	1.863263871	1.724520167	2.4788552	+
GPRC5A	3.266811021	3.568735553	1.552097836	+
HPGD	1.69985419	1.953144922	1.539682093	+
HSD3B1	2.358187611	1.695748245	1.524467612	+
IGFL2	3.201749638	2.005281117	1.807112096	-
IQGAP2	2.336867604	3.422090705	3.492051898	+
ITGA2	2.617969882	2.910492904	1.724110212	+
ITGA3	2.362826176	2.853847017	1.501348603	+
KIAA0040	2.634706942	2.820649686	1.504893612	+
LST-3TM12	2.672372281	2.875858115	1.885372382	+
MID1	2.470302984	2.345999978	1.502697378	+
MOSPD1	2.246864308	2.478968604	1.963937475	+
MPP1	2.321544604	1.544007756	2.867735568	+
MT1G	1.526823715	1.981310515	1.575495354	+
MT2A	1.468379624	1.741433039	1.825776284	+
NOSTRIN	3.163697145	3.063008775	1.714232744	+
PBX3	2.203468084	1.90449698	1.855082052	+
PHLDB2	2.280591415	2.54587573	1.624053321	+
PPP4R1L	1.761186267	1.753157366	1.728356109	+
RGL1	1.555617101	1.546234893	1.734921035	+
ROR1	1.747773218	1.581259887	1.505649537	+
SCEL	1.879505973	2.029396832	3.321397747	+
SCML1	1.822943061	2.51213762	1.519873234	-
SEMA3C	5.200343784	6.227935486	2.458712417	+
SERPINA1	1.68752924	1.611616521	1.540034318	+
SERPINE2	1.807806793	2.420141666	1.541170525	-
SLC7A7	7.153719248	4.938549943	3.216718078	+
SLCO1B3	5.526405792	6.019929118	2.100467553	-
TNFAIP3	1.889701026	2.189731529	1.791377635	-
TNFRSF9	2.927002545	3.675938169	2.040955179	+
TRIM16	2.076082104	2.439234566	1.502473973	+
VGLL3	1.774237325	2.024405782	3.72883252	-

Table S1, related to Figure 7. Potential target genes of PROX1 in DLD1 and SW480R cells. Combined targets of the microarrays presented in Tables S2 and S3.

Table S2, related to Table S1 (separated file). Genes differentially expressed in SW480R after PROX1 knock-down. Microarray. Cutoff 1.5 fold change, FDR<0.05. See also Table S1.

Table S3, related to Table S1 (separated file). Genes differentially expressed in DLD1-PROX1 vs. DLD1 control cells. Microarray. Cutoff 1.5 fold change, FDR<0.05. See also Table S1.

Supplemental Experimental Procedures

Human tumor samples used for the analysis

The three primary tumor and metastases series were analyzed: 15 primary tumors, 14 lymph nodes and 8 liver metastases (series 1, scored by H.B.); 13 primary tumors, 6 liver metastases, 14 lung metastases, 1 brain metastasis, 1 adrenal gland metastasis, 1 ovarian metastasis, 1 bronchial metastasis and 2 lymph nodes (series 2, scored by I.L.); 5 primary tumors and 5 lung metastases (series 3, scored by I.L.), see the table below for more detailed information. For markers colocalization, slides were also stained for EPHB2, CD44, BMI1 and Keratin 20. Staining for phosphohistone H3 protein was performed on 7 primary tumors, for which at least one lung and liver metastases were available. Lymphatic endothelial cells, which high levels PROX1 (Wigle and Oliver, 1999) were used as an internal positive control. The score represents the percentage of cancer cells with nuclear PROX1 higher or comparable to lymphatic endothelial cells on the same slide. A global percentage ≤5% was considered as negative.

Metastases N°			Metastasis				Analysis	Analysis
Series 1	**Patient ID**	**TNM**	**Liver**	**Lung**	**Lymph N.**	**Others**	PH3	SC
1	H1001332	T3	1	0	1	-	-	-
2	H1007751	T3	1	0	1	-	-	-
3	H0904002	T3	1	0	0	-	-	-
4	H0909081	T3	1	0	1	-	-	-
5	H0904539	T3	1	0	0	-	-	-
6	H0904001	T3	1	0	0	-	-	-
7	H0910992	T3	1	0	0	-	-	-
8	H0912652	T3	1	0	0	-	-	-
9	H0915774	T3	0	0	2	-	-	-
10	11H03026	T3	0	0	2	-	-	-
11	10H7110	T3	0	0	2	-	-	-
12	09H13383	T3	0	0	2	-	-	-
13	09H12474	T3	0	0	1	-	-	-
14	09H7432	T3	0	0	1	-	-	-
15	08H1305	T3	0	0	1	-	-	-
Series 2								
1	4	T1M0N0	0	2	0	-	Yes	-
2	5	T3M0N0	0	0	1	-	-	-
3	6	T3M1N1	0	1	0	Brain	-	-
4	7	T2M0N0	0	1	0	-	-	-
5	8	T3M0N0	1	1	0	-	Yes	-
6	15	T3M0N0	0	1	0	Bronchial	-	-
7	17	T3M0N1	1	1	0	-	Yes	-
8	18	T3M1N0	0	1	1	-	-	-
9	19	T1M0N0	1	1	0	-	Yes	-
10	22	T3M0N0	1	1	0	-	Yes	-
11	23	T3M2N1	1	3	0	-	Yes	-
12	27	T2M0N0	0	0	0	Adrenal Gland	-	-
13	29	T4M2N1	1	1	0	Ovary	Yes	-
Series 3								
1	Case1	T3N1	0	1	0	-	-	Yes
2	Case2	T3N0	0	1	0	-	-	Yes
3	Case3	T3N0	0	1	0	-	-	Yes
4	Case4	T3N1	0	1	0	-	-	Yes
5	Case5	T2N0M1	0	1	0	-	-	Yes

Table S4, related to Figure 1. Human tumor and metastasis series samples used.

The samples are related to data presented in Figures 1 and S1.

Bioinformatics analyses of published data sets.

Statistical significance of differences in correlation values between lung metastasis and primary tumors was assessed by a permutation test. To study the expression of genes or gene signatures, primary tumor and lung metastasis samples were divided in 3 categories by tertiles of PROX1 expression level (high, medium and low). The number of samples per group were: Lung 7 high, 6 med, 7 low; Primary 63 high, 61 med, 62 low. Average expression of single genes or signatures in spider graphs was plotted in log scale. The grey inner circle delimits the level of the average expression across the 6 categories.

Analyses of PROX1 expression in CRC subtypes

Budinska et al. reported that unsupervised clustering based on gene modules lead to distinguish five different gene expression CRC subtypes (A to E, (Budinska et al., 2013)). We also applied the subtype system of (Sadanandam et al., 2013) to the PETACC-3 (Pan-European Trials in Alimentary Tract Cancers) database, containing histopathological evaluation, mutation analysis and MSI status analysis for 688 stage II/III human CRC primary tumors (Roth et al., 2010). Gene expression with the ALMAC Colorectal Cancer DSA platform (Craigavon, Northern Ireland), a customized Affymetrix chip with 61,528 probe sets mapping to 15,920 unique Entrez Gene IDs, was reported in (Popovici et al., 2012). In this case, Sadanandam et al. algorithm separated tumors into stem-like, Goblet cells and inflammatory subtypes, while transient-amplifying and enterocytes signatures remained merged together (N.Zangger, unpublished observation). Wilcoxon rank test was computed to assess statistical significance.

Correlation of PROX1 levels with MSS and MSI status in CRC

For the analysis of PROX1 mRNA levels in human normal colon, colorectal adenomas, and MMR^+ and MMR^- CRCs and cell lines, expression data were extracted from a published microarray dataset (Sabates-Bellver et al., 2007). The tissue groups were composed of 32 normal mucosae samples, 32 adenomas, 13 MMR^+ CRCs and 12 MMR^- CRCs. The CI of the qPCR was 0.05. For the analysis of PROX1 protein level in MMR^+ vs. MMR^- tumors, 160 human CRCs samples were stained for PROX1, ß-catenin (CTNNB1) or CMYC, and scored by F.B. The MMR status was evaluated by staining adjacent sections for the mismatch repair MLH1 or MSH2 proteins. Global correlation of PROX1 expression levels with the microsatellite status and other pathological and molecular parameters was performed using the PETAC-3 database, which contains histopathological evaluation, mutation analysis, and MSI or MSS status for 688 human stage II/III CRCs (Roth et al., 2010). Gene expressions was measured on the ALMAC Colorectal Cancer DSA platform (Craigavon, Northern Ireland), a customized Affymetrix chip with 61,528 probe sets mapping to 15,920 unique Entrez Gene IDs, as described in (Popovici et al., 2012). MSI status was determined using a panel of 10 mononucleotide and dinucleotide microsatellite loci by polymerase chain reaction amplification of normal/tumor DNA pairs. MSI was graded as high (MSI-H) or low (MSI-L) (Roth et al., 2010).

Production of cell lines and cell culture procedures

shProx1 or shBcl2l15 intestinal $Apc^{f/f};Kras^{G12D};Tp53^{f/f}$ organoids were produced by transducing cells with lentiviruses encoding PROX1shRNA and control scrambled shRNA in pLL3.7 backbone, described previously (Petrova et al., 2008). Organoids were dissociated and GFP^+ cells sorted and plated for the clonogenic assay.

Alternatively, mouse scrambled (TRC PLKO.1), mouse Prox1 (CloneId, TRCN0000070725, Thermo Scientific) or mouse Bcl2l15 shRNA (1RMM4431-200308443, Thermo Scientific) were used for organoid transduction, which were then selected with puromycin (3µg/ml) for 10 days before dissociation and clonogenic assay or transplantation. SW620 shPROX1 and shCtr cells were produced by transducing cells with recombinant lentiviruses expressing PROX1shRNA and control scrambled shRNA, described previously (Petrova et al., 2008). For target gene overexpression, cDNAs were subcloned into lentiviral vector pSD44 and used for the productition of stably transduced pools. SW480A, SW480R/PROX1si and SW480R/GFPsi cell lines were described previously (Petrova et al., 2008). For overexpression experiments, PROX1 wild type and mutated (N625A) PROX1 cDNAs (Petrova et al., 2002) were subcloned into lentiviral vector pSD44, DLD1 cells were transduced with PROX1, PROX1mut or control lentiviruses and pools of cells were produced using puromycin selection. Alternatively, individual DLD1 clones were generated using stable transfection of PROX1-pAMC and PROX1N625A-pAMC plasmids (Petrova et al., 2002), followed by selection in 250µg/ml geneticin (Gibco). Primary tumor growth and formation of metastases was similar in pools and individual clones. To facilitate detection, cells were tagged with firefly luciferase (DLD1 or SW480R cells), or EGFP (SW620 cells). All cell lines were monitored routinely for PROX1 expression level by Western blotting, and discarded and freshly thawed every 4 months, or earlier if notable changes in PROX1 expression were observed.

For clonogenic assay, cell were isolated after 4 days induction with tamoxifen 1mg/g/day (Sigma) from the intestinal epithelium of *Apc$^{f/f}$;Kras^{G12D};Tp53$^{f/f}$;villin-*

CreERT2 mice as described (Sato et al., 2011) and transduced. For lentiviral transduction, $1x10^5$ dissociated *AKP* cells were transduced with the control, Prox1 or Bcl2l15 targeting shRNAs. The transduction was performed under spinning for 1 hour, plus 6 hours at 37°C with 5%CO_2, followed by a recover in Matrigel (Corning, 356231) for 3 days. For selection, the cells were either sorted by FACS to isolate GFP^+ transduced cells or maintained in 3µg/ml puromycin in DMEM/F12, 1x Glutamax, Hepes 0.01M, B27 and N2 1x (Gibco). In all cases, knock-down was confirmed by qPCR and staining. For the clonogenic assay, the organoids were dissociated, 3000 single cells/well were plated in 50µl Matrigel and cultured for 15 days in Advanced DMEM/F-12 (Gibco) with 1x N-2 and B-27 (Gibco), glutamine 1% and Hepes 0.01M (Gibco) before quantification.

SW620 cells were maintained in complete RPMI and 15 µg/ml Puromycin (Sigma). SW480R cells were maintained in 50 µg/ml Zeocin (Invitrogen) and 10 µg/ml Blasticidin (Gibco) and complete RPMI. For western blot analysis we plated $4x10^5$ on 6 well plate dishes (final protein concentration measured with BCA assay, Roche), for RNA extraction $2x10^6$ cells on p100 petri dishes, for cell stainings $2x10^5$ cells on coverslips inserted in 24well plates, or $0.5x10^5$ cells on 8 well chambers (Costar), for Trypan Blue counting $5x10^4$ cells on 48 well plates, and for cell titer blue (CTB, Promega), and CyQuant NF analysis (Invitrogen) $6x10^3$ cells on 96 well plates. RNA and proteins were isolated at 12, 24 and 48 hours.

For the analysis of spheroids, $3.5x10^3$ cells were seeded in the MMP-Degradable synthetic extracellular MT3D Matrix functionalized with RGD peptides (QGelBio) and cultured for 21 days. For spheroid growth quantification 5 random pictures were

acquired from every well using a phase contrast inverted microscope (Axio Observer.Z1). At the end of the experiment, the disks were incubated for 1h in 200µM pimonidazole (Hypoxyprobe™-1 kit, HPI), washed twice in cold PBS, fixed for 4 hours in 4% PFA and processed for whole mount staining or embedded in OCT and sectioned for immunohistochemical staining. Images of spheroids were acquired using a Zeiss LSM 510 Meta inverted confocal microscope**.** For $TUNEL^+$ cell quantification cells were counted and normalized by the total number of $DAPI^+$ cells in single sections. 15 spheres or 3 slides from different depths were used for every cell type. For phosphohistone $H3^+$ quantification 10 entire spheres were reconstructed with Z stacks images per condition.

Cell invasion assays were performed using $5x10^4$ cells/well in 24-well plates with 8µm pore size inserts (Costar, 6.5mm diameter, 8µm pore size) uncoated or coated with 2mg/ml or 3.5mg/ml Matrigel for DLD1 or SW620 cells, respectively. Complete RPMI with 10% FBS was used as chemo-attractant after 24 hours starvation. Each condition was done in triplicate, and 3 pictures from every membrane were used for quantification. Similar results were observed in two independent experiments.

For hypoxia and nutrient deprivation experiments, the cells were incubated in a hypoxic chamber (Billups-Rothenberg) in 0.1% O_2 or in normoxia. DMEM with no glucose and pyruvate (Gibco 31966-021), DMEM without glutamine and pyruvate (Gibco 11966-025) or DMEM with glutamine and pyruvate (Gibco 11960-044) supplemented with 10% FBS were used as culture media. After 72 hours, live cell number was determined using CyQuant NF (Invitrogen) DNA-based assay.

Chloroquine (CQ, 5µM), 3–methyadenine (3-MA, 1mM), or etoposide were added 12 hours after plating.

Animal experiments.

We used 8 to 12 week-old NOD-scid; *IL-2Rγ*$^{-/-}$ mice for tumor xenograft experiments. The *Apc*$^{fl/fl}$ mice (Sansom et al., 2004; Shibata et al., 1997) were crossed with *Lgr5-EGFP-CreERT2* mice (Schepers et al., 2012) or *Kras*$^{Lsl\text{-}G12D}$ (Jackson et al., 2001), *Tp53*$^{fl/fl}$ (Marino et al., 2000) and *villin-CreERT2* mice (el Marjou et al., 2004) to obtain *Apc*$^{fl/fl}$*;Lgr5-EGFP-CreERT2* or *Apc*$^{fl/fl}$*;Kras*$^{Lsl\text{-}G12D}$*;Tp53*$^{fl/fl}$*;villin-CreERT2* (*AKP*) animals. To generate adenomas and tumors for histological analysis, in *Apc*$^{fl/+}$*; Lgr5-EGFP-CreERT2* and *Apc*$^{fl/+}$*;Kras*$^{Lsl\text{-}G12D}$*;Tp53*$^{fl/fl}$*;villin-CreERT2* mice, the Cre recombinase was activated by a single 1mg/20g mouse i.p. injection of tamoxifen. The tumors were analyzed after 24 days (n=4), and mice were injected i.p. with EdU (Invitrogen) 2 hours prior to sacrifice.

In order to obtained fresh intestinal tumorigenic organoids to culture *in vitro*, 2 *Apc*$^{fl/fl}$*;Kras*$^{Lsl\text{-}G12D}$*;Tp53*$^{fl/fl}$*;villin-CreERT2* mice were injected daily with tamoxifen 1mg/20g. After 4 days from the first injection, the intestinal crypts were isolated and cultured in Matrigel (Corning, 356231) as described previously (Sato et al., 2011).

For orthotopic models, 1x10^6 cells suspended in 25µl RMPI containing 33% Matrigel (BD) were injected in caecum as previously described (Cespedes et al., 2007; Zaric et al., 2012), using a 50µl 28G syringe (Hamilton). When indicated, tumor growth was monitored by *in vivo* bioluminescence after i.p. Injection of 1.5mg/g luciferin (Biosynth), using IVIS Lumina II (Xenogen). PROX1$^+$ vs. PROX1$^-$ luciferase-

transduced cells had similar level of luciferase activity *in vitro* (data not shown). For inducible knockdown experiments, SW480R/PROX1si and SW480R/GFPsi lines, which express PROX1 or GFP targeting shRNA upon doxycycline addition, were used (Petrova et al., 2008). Doxycycline hyclate 2.5mg/ml (Sigma) was administered in drinking water supplemented with 10% sucrose at the day of tumor implantation. Control group mice received water with 10% sucrose. For PROX1 suppression in established metastases, a group of SW480R/PROX1si injected mice were randomized at day 30 to receive doxycycline or sucrose only. The time point was selected because a stable bioluminescent signal from metastases, determined as two consecutive positive measurements in 7 days, was observed in every mouse. At the time of sacrifice *ex vivo* bioluminescence (DLD1, SW480R) or EGFP fluorescence (SW620) was analyzed in organs and in primary tumor using IVIS Lumina II or Leica M205FA stereomicroscope. For *ex vivo* bioluminescence mice were injected with luciferin 15 minutes prior to sacrifice and dissected organs were immersed in PBS containing 0.15mg /ml of luciferin.

For the lung colonization assay, mice survival analysis and CQ treatment, $1x10^5$ SW620 shPROX1 or shCtr cells in 100µl PBS were injected into tail vein (n=11-12 per group). For lung colonization assay mice were sacrificed after 2.5 and 7 days, perfused intracardially with PBS and tissues were prepared and analyzed as described above. For the survival study, mice were sacrificed when becoming moribund according to institutional guidelines. For CQ treatment, mice were randomized at day 3 or 7 after tumor cell injection to receive 40 or 10 mg/kg CQ or PBS I.P. daily. After orthotopic implantation, 10mg/kg/day treatment has been followed, starting from day 15.

For intestinal organoid implantation, organoids were dissociated and plated in matrigel at 6000 cells density. After 3 days in culture, the organoids were collected from Matrigel with a cell recovery solution (Corning), stained with trypan blue and counted. The spheres were then resuspended in Matrigel/advanced DMEM/F12 (50/50), and 50 spheroids/mouse were implanted with a 20G needle.

Staining procedures and list of primary antibodies.

Tissues were fixed in 4% paraformaldehyde (PFA) and embedded in paraffin. 5µm deparaffinized sections were subjected to heat-induced epitope retrieval (High/Low pH Retrieval solution, DAKO). qGel disks containing spheroids were fixed in 4% PFA and processed for whole mount staining or embedded in OCT to obtain 6µm frozen sections. Frozen sections were fixed in -20°C cold 50% MetOH-50% Acetone (Fluka). Cultured cells were fixed with 4% PFA and permeabilized with 0.5% Triton X-100. Alexa Fluor fluorochrome-conjugated secondary antibodies (Invitrogen) were used in fluorescent stainings; biotinylated IgG (Vector) were used together with the TSA™ kit (PerkinElmer) for chromogenic detection.

The following antibodies and dyes were used for staining and Western blot analyses: rabbit anti-human BCL2L15 (Atlas antibodies); mouse anti-human BMI1 (Abcam); rabbit anti-activated Caspase 3 (Asp175, Cell Signaling); rat anti-mouse CD44 (BD Pharmigen™); rat anti-mouse endomucin (eBioscience), goat anti-mouse EphB2 (AF467, R&D Systems), FITC-conjugated phalloidin (Invitrogen), rabbit anti-GFP (ab290, Abcam); mouse anti-human Glut1 (SPM498, Thermo Scientific); rabbit anti-human HIF-1α (10006421, Cayman); mouse anti-human Ki67 (BD Pharmigen™);

rabbit anti-mouse Keratin 6 (Covance); mouse anti-human Keratin 20 (Ks20.8, Dako); rabbit anti-human LC3B (ab51520, Abcam); rabbit anti-human lysozyme (Dako); rabbit anti–human phosphohistone H3 (Ser10 D2C8, Cell Signaling), rabbit anti-pimonidazole adducts (HPI, 4.3.11.3, Hypoxyprobe) ; goat anti-human PROX1 (AF2727, R&D), rabbit anti-human PROX1 (Abcam); TUNEL (4815-30-K, Chromogenic R&D Systems Ready Kit); mouse anti-human Vimentin (V9, DakoCytomation); mouse anti-human β-Catenin (14, aa.571-781, BD Transduction LaboratoriesTM); EdU detection kit (Click It, Invitrogen); mouse anti-human ß-actin (C11, Sigma-Aldrich), mouse anti-human GAPDH (G9545, Sigma-Aldrich); mouse anti-human E-Cadherin (24E10, Cell Signaling).

Gene expression profiling analysis.

The following PROX1 siRNA were used for silencing: 5'-CCG AGU GCG GCG AUC UUC AAG AUA U-3' (PROX1HSS108596, Invitrogen), 5'-GGC CUA CUA UGA GCC AGU UUG AUA U-3' (PROX1HSS108597, Invitrogen). At least 90% downredulation of PROX1 protein was observed by Western blot analysis by either PROX1 siRNA but not the control siRNA (not shown) at the time of RNA collection. Affymetrix Human Gene 1.0 ST arrays (Affymetrix) were hybridized with 2.7μg of biotinylated target at 45°C for 17 hours washed and stained according to the protocol described in Affymetrix GeneChip® Expression Analysis Manual (Fluidics protocol FS450_0007). The arrays were scanned using the GeneChip® Scanner 3000 7G (Affymetrix) and raw data was extracted from the scanned images and analyzed with the Affymetrix Power Tools software package (Affymetrix). All statistical analyses were performed using the high-level interpreted statistical language R and various Bioconductor packages (http://www.bioconductor.org). Hybridization quality was

assessed using the Expression Console software (Affymetrix). Normalized expression signals were calculated from Affymetrix CEL files using the quantile normalization method. Differential hybridized features were identified using Bioconductor package "limma" that implements linear models for microarray data (Smyth, 2004). The P values were adjusted for multiple testing calculating false discovery rates (FDR) with the Benjamini and Hochberg's method (Klipper-Aurbach et al., 1995). Differentially expressed genes were identified by FDR lower than 0.05 and fold change greater than 1.5. Microarray data are deposited in ArrayExpress.

qPCR analyses

Analysis of gene expression was carried out using the comparative Ct (ΔΔCt) method as described by the manufacturer (Fold change 2-ΔΔCt).

List of primers used

ABAT fwd: gac agg gac acc ctt tgc
ABAT rev: gaa gtc gag cag aca ccc a
ANXA6 fwd: ctg gtt tgg cca tgg tct c
ANXA6 rev: gtt gct gct ggg cta acg
ASCL2 fwd: ctc gcc ctc ccg cgg ttc tt
ASCL2 rev: cca gca gtg tcc ctc cag cag
Ascl2 fwd: aag cac acc ttg act ggt acg
Ascl2 rev: aag tgg acg ttt gca cct tca
BCL2L15 fwd: aac cat taa ggg aca gac agg a
BCL2L15 rev: gcc acc tgt ccc act act tc
Bcl2l15 fwd: aca ggc agg aag tac tgt act caa
Bcl2l15 rev: atg ccc gtc acg tag tta gc
CAV1 fwd: tcc ctt ctg gtt ctg caa tc
CAV1 rev: cga gaa gca agt gta cga cg
EPHB2 fwd: aga aac gct aat gga ctc cac t
EPHB2 rev: gtg cgg atc gtg ttc atg tt
EphB2 fwd: gcg gct acg acg aga aca t
EphB2 rev: ggc taa gtc aaa atc agc ctc a
GPRC5A fwd: cat ttt cag ctg cag aac ca
GPRC5A rev: gag gca aac tgt tcc cgt ag
IQGAP2 fwd: att cag tgg ttg gtg gca a
IQGAP2 rev: tct gca gag gag atg gat ga
LGR5 fwd: ctc cca ggt ctg gtg tgt tg
LGR5 rev: gag gtc tag gta gga ggt gaa g
Lrg5 fwd: cct act cga aga ctt acc cag t
Lrg5 rev: gca ttg ggg tga atg ata gca
RNF43 fwd: cat cag cat cgt caa gct gga
RNF43 rev: tta ccc cag atc aac acc act
Rnf43 fwd: tcc gaa aga tca gca gaa cag a
Rnf43 rev: gga ctg cat tag ctt ccc ttc
TNFRSF9 fwd: ctt ctt ctg gaa atc ggc ag
TNFRSF9 rev: acg ctc cgt ttc tct gtt gt
GAPDH fwd: aac gtg tca gtg gtg gac ctg acc t
GAPDH rev: gtc gtt gag ggc aat gcc agc ccc a
18S fwd: agg aat tcc cag taa gtg cg
18S rev: gcc tca cta aac cat cca a

PROX1 ChIP-seq

SW480R cells were cross-linked with formaldehyde, chromatin was fragmented using SimpleChIP Enzymatic Chromatin IP Kits (Cell Signaling) and immunoprecipitated using goat anti–human PROX1 antibody (R&D Systems) complexed with protein G Sepharose. 10ng of ChIP sample was quantified using the Qubit fluorometer (Invitrogen) and DNA were prepared using the ChIP-Seq Sample Preparation Kit (Illumina) according to the manufacturer's protocol. Libraries were sequenced on the Illumina Genome Analyzer IIx using the Single-Read Cluster Generation Kit v4 and 38 Cycle Sequencing Kit v4. Data were processed using the Illumina Pipeline Software v1.60. The aligned sequences were generated using the ELAND module within the Illumina Genome Analyzer Pipeline Software, v1.3 (Illumina, Inc.) and mapped to the assembly 18 of human genome. Transcription factor binding sites were identified using SISSRs (Site Identification from Short Sequence Reads) (Jothi et al., 2008). To reduce false positive calls, DNA input was used as a control channel in SISSRs. CEAS (Ji et al., 2006) was used to detect nearest Ref Seq genes and position of binding sites, as indicated in the main text.

BCL2L15/PROX1 correlation statistical analysis

230 MSS primary tumors and 17 normal tissues (TCGA database project: http://cancergenome.nih.gov/) were analyzed. Two-sample Wilcoxon test on normal tissue versus CRC was significant for both genes (PROX1, P=4.45e-08; BCL2L15 P=2.25e-06). Spearman correlation between the two genes was not significant in normal tissue (P=0.63) due to the absence of PROX1 expression, but significant for tumor samples (P=1.8e-04).

Generation of BCL2L15 reporters and luciferase assay

To generate *BCL2L15* reporters, we amplified four 200bp fragments from the center of the peaks in *BCL2L15* locus in and cloned them into pTA-luc vector (Clontech). The genomic coordinates (human genome 18) of the fragments and the primers used for amplifications are as follows :

Reporter 1:
chr1: 114200350-114200550
Primer 1 ACAGGTTTTTGCCATGTC
Primer 2 ACTCTAAAAGTTAAGTTCAATAGTG

Reporter 2:
chr1: 114215750-114216950
Primer 1 GAATTTCTCTTTGGTCCATG
Primer 2 GACCACAGAAGGTGGTTA

Reporter 3:
chr1: 114218800-114219000
Primer 1 AAACATTTTGCCAGAACCAT
Primer 2 ATTTCCCCTTAAACTAGCAT

Reporter 4:
chr1: 114232100-114232300
Primer 1 AAATGAGTAATCGCATTGTT
Primer 2 AGTGTTATGCCTCCTTTTTG

For luciferase assays, SW480 cells were cultured in 24-well-plates and transfected by using jetPEI transfection reagent (Polyplus Transfection) following manufacturer's instruction. Renilla luciferase reporter CMV-RL (Norrmen et al., 2009) was co-transfected for normalization. 48 h after the transfection cell were lysed and analyzed for luciferase activity using the Dual-LuciferaseTM kit (Promega).

Statistical analyses

Pairwise comparisons were performed by two-tailed Student's t test. Recurrence of the metastases, lung colonization assay data, grouped analysis over time and other multiple populations analysis were analyzed through a Two-way ANOVA followed by Bonferroni post-tests. Multiple groups were analyzed over one variable with One-way ANOVA (non parametric) with Bartlett's test for equal variances and Tukey post-tests to compare each group independently. For overall survival analysis, the Kaplan-Meyer method was used. Similar results were obtained using the Log-rank (Mantel-Cox) test or the Gehan-Breslow-Wilcoxon test.

Column or grouped analysis data were represented as vertical box & whiskers, where error whiskers had Tukey appearance; vertical mean and standard mean error (SEM) plus replicates; or histograms with vertical bars indicating the mean ± SEM. Each *in vitro* or 3D culture experiment was repeated at least twice independently.

Supplemental References

Budinska, E., Popovici, V., Tejpar, S., D'Ario, G., Lapique, N., Sikora, K. O., Di Narzo, A. F., Yan, P., Hodgson, J. G., Weinrich, S.*, et al.* (2013). Gene expression patterns unveil a new level of molecular heterogeneity in colorectal cancer. J Pathol.

Cespedes, M. V., Espina, C., Garcia-Cabezas, M. A., Trias, M., Boluda, A., del Pulgar, M. T., Sancho, F. J., Nistal, M., Lacal, J. C., and Mangues, R. (2007). Orthotopic microinjection of human colon cancer cells in nude mice induces tumor foci in all clinically relevant metastatic sites. Am J Pathol *170*, 1077-1085.

el Marjou, F., Janssen, K. P., Chang, B. H., Li, M., Hindie, V., Chan, L., Louvard, D., Chambon, P., Metzger, D., and Robine, S. (2004). Tissue-specific and inducible Cre-mediated recombination in the gut epithelium. Genesis *39*, 186-193.

Jackson, E. L., Willis, N., Mercer, K., Bronson, R. T., Crowley, D., Montoya, R., Jacks, T., and Tuveson, D. A. (2001). Analysis of lung tumor initiation and progression using conditional expression of oncogenic K-ras. Genes Dev *15*, 3243-3248.

Ji, X., Li, W., Song, J., Wei, L., and Liu, X. S. (2006). CEAS: cis-regulatory element annotation system. Nucleic Acids Res *34*, W551-554.

Jothi, R., Cuddapah, S., Barski, A., Cui, K., and Zhao, K. (2008). Genome-wide identification of in vivo protein-DNA binding sites from ChIP-Seq data. Nucleic Acids Res *36*, 5221-5231.

Klipper-Aurbach, Y., Wasserman, M., Braunspiegel-Weintrob, N., Borstein, D., Peleg, S., Assa, S., Karp, M., Benjamini, Y., Hochberg, Y., and Laron, Z. (1995). Mathematical formulae for the prediction of the residual beta cell function during the first two years of disease in children and adolescents with insulin-dependent diabetes mellitus. Med Hypotheses *45*, 486-490.

Marino, S., Vooijs, M., van Der Gulden, H., Jonkers, J., and Berns, A. (2000). Induction of medulloblastomas in p53-null mutant mice by somatic inactivation of Rb in the external granular layer cells of the cerebellum. Genes Dev *14*, 994-1004.

Norrmen, C., Ivanov, K. I., Cheng, J., Zangger, N., Delorenzi, M., Jaquet, M., Miura, N., Puolakkainen, P., Horsley, V., Hu, J.*, et al.* (2009). FOXC2 controls formation and maturation of lymphatic collecting vessels through cooperation with NFATc1. J Cell Biol *185*, 439-457.

Petrova, T. V., Makinen, T., Makela, T. P., Saarela, J., Virtanen, I., Ferrell, R. E., Finegold, D. N., Kerjaschki, D., Yla-Herttuala, S., and Alitalo, K. (2002). Lymphatic endothelial reprogramming of vascular endothelial cells by the Prox-1 homeobox transcription factor. Embo J *21*, 4593-4599.

Petrova, T. V., Nykanen, A., Norrmen, C., Ivanov, K. I., Andersson, L. C., Haglund, C., Puolakkainen, P., Wempe, F., von Melchner, H., Gradwohl, G.*, et al.* (2008). Transcription factor PROX1 induces colon cancer progression by promoting the transition from benign to highly dysplastic phenotype. Cancer Cell *13*, 407-419.

Popovici, V., Budinska, E., Tejpar, S., Weinrich, S., Estrella, H., Hodgson, G., Van Cutsem, E., Xie, T., Bosman, F. T., Roth, A. D., and Delorenzi, M. (2012). Identification of a poor-prognosis BRAF-mutant-like population of patients with colon cancer. J Clin Oncol *30*, 1288-1295.

Roth, A. D., Tejpar, S., Delorenzi, M., Yan, P., Fiocca, R., Klingbiel, D., Dietrich, D., Biesmans, B., Bodoky, G., Barone, C.*, et al.* (2010). Prognostic role of KRAS and BRAF in stage II and III resected colon cancer: results of the translational study on the PETACC-3, EORTC 40993, SAKK 60-00 trial. Journal of clinical oncology : official journal of the American Society of Clinical Oncology *28*, 466-474.

Sabates-Bellver, J., Van der Flier, L. G., de Palo, M., Cattaneo, E., Maake, C., Rehrauer, H., Laczko, E., Kurowski, M. A., Bujnicki, J. M., Menigatti, M.*, et al.* (2007). Transcriptome profile of human colorectal adenomas. Molecular cancer research : MCR *5*, 1263-1275.

Sadanandam, A., Lyssiotis, C. A., Homicsko, K., Collisson, E. A., Gibb, W. J., Wullschleger, S., Ostos, L. C., Lannon, W. A., Grotzinger, C., Del Rio, M.*, et al.* (2013). A colorectal cancer classification system that associates cellular phenotype and responses to therapy. Nat Med *19*, 619-625.

Sansom, O. J., Reed, K. R., Hayes, A. J., Ireland, H., Brinkmann, H., Newton, I. P., Batlle, E., Simon-Assmann, P., Clevers, H., Nathke, I. S.*, et al.* (2004). Loss of Apc in vivo immediately perturbs Wnt signaling, differentiation, and migration. Genes Dev *18*, 1385-1390.

Sato, T., Stange, D. E., Ferrante, M., Vries, R. G., Van Es, J. H., Van den Brink, S., Van Houdt, W. J., Pronk, A., Van Gorp, J., Siersema, P. D., and Clevers, H. (2011). Long-term expansion of epithelial organoids from human colon, adenoma, adenocarcinoma, and Barrett's epithelium. Gastroenterology *141*, 1762-1772.

Schepers, A. G., Snippert, H. J., Stange, D. E., van den Born, M., van Es, J. H., van de Wetering, M., and Clevers, H. (2012). Lineage tracing reveals Lgr5+ stem cell activity in mouse intestinal adenomas. Science *337*, 730-735.

Shibata, H., Toyama, K., Shioya, H., Ito, M., Hirota, M., Hasegawa, S., Matsumoto, H., Takano, H., Akiyama, T., Toyoshima, K.*, et al.* (1997). Rapid colorectal adenoma formation initiated by conditional targeting of the Apc gene. Science *278*, 120-123.

Smyth, G. K. (2004). Linear models and empirical bayes methods for assessing differential expression in microarray experiments. Stat Appl Genet Mol Biol *3*, Article3.

Wigle, J. T., and Oliver, G. (1999). Prox1 function is required for the development of the murine lymphatic system. Cell *98*, 769-778.

Zaric, J., Joseph, J. M., Tercier, S., Sengstag, T., Ponsonnet, L., Delorenzi, M., and Ruegg, C. (2012). Identification of MAGI1 as a tumor-suppressor protein induced by cyclooxygenase-2 inhibitors in colorectal cancer cells. Oncogene *31*, 48-59.